ABSTRACT

Title of Thesis: DYNAMIC MODELING OF VAPOR COMPRESSION SYSTEMS FOR RESIDENTIAL HEAT PUMP APPLICATIONS WITH ALTERNATIVE LOW-GWP REFRIGERANTS

Viren Bhanot
Master of Science, 2015

Thesis Directed By: Dr. Reinhard Radermacher, Professor
Department of Mechanical Engineering

Dr. Yunho Hwang, Research Professor
Department of Mechanical Engineering

With the increased focus on reducing greenhouse gas emissions, low-GWP refrigerants, R32 and D2Y60, have been proposed as drop-in replacements for R410A in residential heat pumps. This thesis presents the development of a modeling framework in Simulink® for the dynamic simulations of such residential heat pumps. The framework is component-based, allowing arbitrary cycle configurations, and includes most of the relevant components. Finite-volume method has been applied to the heat exchanger. Compression and expansion processes are treated as quasi-steady

state. The framework has been used to study the performance of the system using the baseline refrigerant and charge-optimized alternatives at ASHRAE test conditions, and the results have been compared against experimental data. Steady-state COP values fall within ±8% of experimental data. For the cyclic tests, the pressure and temperature behaviors compare well and accumulated capacity and power consumption errors are found to be within ±9%. Relative differences between the refrigerants are consistent between simulations and measurements. The framework shows potential for being used to simulate the operation of residential heat pumps under dynamic conditions.

DYNAMIC MODELING OF VAPOR COMPRESSION SYSTEMS FOR RESIDENTIAL HEAT PUMP APPLICATIONS WITH ALTERNATIVE LOW-GWP REFRIGERANTS

By

Viren Bhanot

Thesis submitted to the Faculty of the Graduate School of the
University of Maryland, College Park, in partial fulfillment
of the requirements for the degree of
Master of Science
2015

Advisory Committee:
Dr. Yunho Hwang, Chair
Dr. Jelena Srebric
Dr. Bao Yang

Growth for the sake of growth is the ideology of a cancer cell
Edward Abbey

There is more to life than increasing its speed
Mohandas Gandhi

Acknowledgments

I would like to thank my committee chair Professor Yunho Hwang for helping me make this thesis as strong as possible. I would also like to thank the other committee members Professor Jelena Srebric and Professor Bao Yang for taking time out of their busy schedules to help me defend my work.

I also sincerely thank Professor Reinhard Radermacher for giving me this opportunity to get my Master's degree in the US. Thanks to him, I got a chance to work alongside some of the most talented minds of my field, get a graduate degree, and move onto the next stage of my life without the dark cloud of student debt. Many thanks also go to Dr. Vikrant Aute for taking me through the paces of what it means to be a good researcher. Despite working, as we like to say in the lab, 25 hours a day, he manages to lend a patient listening ear and offer good advice when one turns to him.

In the world of research, it is common knowledge that a five-minute conversation with a coworker can do more to clear up doubts than large stacks of books can. In my case, three colleagues who have really helped me understand the field are Daniel Bacellar, Dr. Hongtao Qiao and Dr. Jiazhen Ling. I feel fortunate to be able to call them colleagues.

Also, despite being thickheaded about personal relationships, I've somehow managed to maintain friendships that have been invaluable in helping me get through the two years at Maryland, so thank you to all. Lastly, my mother, father and brother have all been forgiveness personified in the face of an absentee son/brother who seems to call only when a crisis has erupted. Thank you for being so patient, understanding and loving. I only wish I could be half as generous in return.

Table of Contents

List of Tables

List of Figures

Nomenclature

Symbols

A	area [m^2]
a	curve fit coefficient
b	curve fit coefficient
c	curve fit coefficient
C_p	specific heat capacity at constant pressure (J kg^{-1} K^{-1})
C_v	valve flow coefficient [-]
DAE	Differential Algebraic Equations
f	function of state variables [-]
f	friction factor [-]
F	spring force [N]
FPM	fins per meter [m^{-1}]
G	valve diaphragm balance factor [N m^{-3}]
h	specific enthalpy [J kg^{-1}]
H	height [m]
K	PID gain [-]
L	length [m]
Le	Lewis number [-]
M	mass matrix [-]
$\dot{m}$	mass flow rate [kg s^{-1}]
NBT	number of banks of tubes [-]
NPC	number of parallel coils [-]

NTB	number of tubes per bank [-]
ODE	Ordinary Differential Equations
P	pressure [Pa]
$\dot{Q}$	heat transfer rate [W]
RPM	revolutions per minute [rev^{-1}]
t	time [s]
T	temperature [K]
u	refrigerant velocity [m s^{-1}]
U	vector of state variables [-]
V	specific volume [m^3 kg^{-1}]
V	volume [m^3]
W	Compressor power consumption [W]
x	vapor quality [-] or length along refrigerant flow direction [m]
X	compressor map parameter
Y	length along air flow direction [m]

Greek letters

α	heat transfer coefficient [W m^{-2} K^{-1}]
δ	thickness [m]
ε	emissivity [-]
κ	spring constant [N m^{-1}]
ϕ	diameter [m]
η	efficiency [-]

φ	valve opening fraction [-]
μ	dynamic viscosity [Pa s]
ρ	density [kg m^{-3}]
τ	time constant [s]
ω	humidity ratio [kg H_2O / kg dry air]

Subscript

a	air
acc	accumulator
bulb	sensor bulb
c	collar
comp	compressor
dis	discharge
disp	displacement
econ	economizer port
eff	effective
f	flash point
g	vapor
hor	horizontal
HX	heat exchanger
i	indexing variable [-]
in	inlet
int	intermediate

isen	Isentropic
l	longitudinal
liq	liquid
min	minimum
mix	mixture
o	outer
orif	orifice
out	outlet
p	proportional or constant pressure or primary
pin	valve pin (head)
r	refrigerant
rev	reverse flow
rod	valve stem
s	secondary or constant entropy
suc	suction
t	transverse
T	transpose (of a matrix)
th	thickness
tp	two phase
vol	volumetric
w	Wall

1 Introduction

1.1 Background and Motivation

The Fifth Assessment Report (AR5) published by the Intergovernmental Panel for Climate Change (IPCC, 2014) asserts that "Human influence on the climate system is clear, and recent anthropogenic emissions of greenhouse gases are the highest in history." The report claims 95% confidence levels that the recent warming trend witnessed over the past few decades has been caused by human activity, warning of "severe, pervasive and irreversible impacts for people and ecosystems" and calling for "…substantial and sustained reductions in greenhouse gas emissions". A sharp reduction in greenhouse gas is clearly an overarching human priority.

According to the Annual Energy Outlook report released by the US Energy Information Administration (US EIA, AEO2015), in the United States, residential energy usage made up about 21% of all energy consumption in 2013, equating to a consumption of 21.10 quads (Quadrillion British Thermal Units), with a delivered energy of 11.32 quads. Space heating and space cooling together account for 5.73 quads, or just over half of delivered energy. Thus, the pursuit of more efficient systems for the conditioning of residential spaces is an area of research that deserves further merit.

Traditionally, air-conditioning units have been used for the cooling of residential spaces, whereas heating has been carried out through the burning of Natural Gas, Fuel Oil or Propane. Direct heating has a maximum coefficient of performance (COP) of 1, where the COP is defined as the output heating or cooling capacity attained per unit of input energy. By contrast, systems operating on the vapor compression cycle (VCC) can have COPs that are several times higher.

Residential heat pumps are vapor compression systems that can perform both cooling and heating of residential spaces using the vapor compression cycle. The most common type of heat pumps are air-source heat pumps, the ductless versions of which are called mini-split heat pumps.

Typical heat pump systems consist of a positive displacement compressor for circulating refrigerant flow, indoor and outdoor air-to-refrigerant heat exchangers for absorbing or rejecting heat, expansion devices, and reversing valves to switch the flow direction when switching from heating to cooling modes. The expansion devices used frequently consist of thermostatic or electronic expansion valves and/or fixed diameter orifices.

Residential heat pumps generally operate using simple thermostat-driven on/off control. Therefore, in practice, they rarely operate under steady-state conditions. The charge migration that occurs during the off-cycle has been shown to cause cycling losses in capacity (Bendapudi, 2008). It is thus important to understand the dynamic behaviors of such systems.

While the dynamic behavior might be evaluated by carrying out experimental testing of a system, it is usually time consuming and expensive to carry out such tests. Numerical simulations give engineers the ability to evaluate the performance of not-yet-existing systems and are much cheaper and faster to perform. Thoroughly-validated simulation tools give engineers the flexibility to compare the performance of multiple cycle configurations and under widely varying operating conditions in a short space of time. In addition, it also provides capabilities for examining different control strategies without needing expensive equipment for such purposes.

1.2 Matlab®/Simulink® Platform

Traditionally, in performing transient simulations of vapor compression systems, engineers have had to develop not just the individual component models and the system solution scheme, but have also had to devise solvers for ordinary differential equations (ODE) or differential algebraic equations (DAE) to integrate the associated governing equations. This requires that the engineers be familiar with the numerical issues that such solvers typically encounter during simulations. While this process allows engineers more control over the overall modeling and simulation, it involves an additional burden of considering not just the physical models but also the numerical issues associated with solving the governing equations.

Using commercially available platforms has the advantage of having well-tested ODE/DAE solvers built-in. Simulink® and Modelica® are two commonly used environments used for transient modeling of physical phenomenon. A recent study (Qiao, 2012) performed a simulation of a 4-component vapor compression system on Simulink®, SimScape™ and Modelica®. The study found that the suction and discharge pressures predicted by all three platforms were very similar to each other, although noted that the computation times were larger for Simulink® and SimScape™ in comparison with Modelica.

Simulink® is extensively used in the industry for modeling and simulation purposes and comes equipped with a suite of ordinary differential equations (ODE) and differential algebraic equations (DAE) solvers for handling both non-stiff and stiff systems. In addition, it is also commonly used for hardware-in-loop simulations as well as controller design. Thus, development of a framework on this platform holds the

promise of being useful beyond the current work for the analysis of more complicated cycles, and the development of novel strategies for control of vapor compression systems.

Some transient modeling tools have been previously developed on the Simulink platform. Thermolib (2009) is a toolbox designed for the analysis of a wide range of thermodynamic systems, ranging from fuel cells, power generation, vapor compression systems etc. However, due to the breadth of its applicability, the individual component models involved are inherently simpler since high-level analysis is of interest rather than detailed component models. As an example, the heat exchanger is treated as a lumped volume.

By contrast, Thermosys (Rasmussen, 2002), originally developed at the University of Illinois, has been designed for the transient simulations of vapor compression systems. The primary goal, however, is controller design for such systems and thus some simplifications have been applied to the individual component models, such as using moving boundary method for modeling the heat exchanger. The toolbox has been applied to several different applications ranging from transportation refrigeration systems (Jain, 2009) to building HVAC systems (Chandan, 2010). In addition, the fluid property calls utilized are through look-up tables generated on a per-fluid basis.

A well-validated framework developed on Simulink® that employs detailed, physics-based models would be useful in conducting research on heat pumps that involves testing alternative fluids as system drop-in replacements, and would also provide a foundation for the simulations of more advanced cycles.

1.3 Literature Review

Interest in the dynamic simulation of vapor compression systems has been steadily growing since the late 1970s, going hand-in-hand with the increasing computing capabilities available to researchers. Lebrun and Bourdouxhe (1998) performed an early review of the modeling methods for dynamic simulations of HVAC equipment. Bendapudi and Braun (2002), as part of an ASHRAE project, performed a literature review of existing dynamic models of vapor compression systems, with a focus on modeling chiller systems. The work reviewed 23 years of modeling efforts, from 1978 to 2001 and concluded that no system model existed that could predict the complete dynamic performance of liquid chillers. More recently, Rasmussen presented a two-part literature review paper (2012a, 2012b) covering commonly used modeling methods and presented a 'tutorial' on employing these typical modeling approaches. The paper documents the limited validations provided in many of the papers reviewed and documents a need for more comprehensive validations of models. Previous work related to individual component models is discussed in the following sections.

1.3.1 Compressor Models

Compressors dictate the mass flow rate of the refrigerant in the vapor compression cycle, along with the expansion device. In evaluating the transient behavior of vapor compression systems, the timescales associated with the variation of compressor mass flow rate are much smaller than heat exchanger dynamics (Winkler, 2009). The compression process is thus often treated as a quasi-steady state phenomenon, with changes in the inlet and outlet conditions instantaneously causing a change in the mass flow rate (Rasmussen, 2012a). A significant number of the models

found in literature also use constant volumetric and isentropic efficiencies to calculate the mass flow rate and outlet enthalpy, respectively.

While most papers treat the compression process as static, several researchers do account for the transients involved in heat transfer through the compressor shell. Eldredge (2006) develops a first-order dynamic model to approximate the compressor shell temperature decay and refrigerant outlet temperature decay during quasi-shutdown conditions, and calculates the time constant using experimental data. Winkler (2009) considers the dynamics of heat transfer from the refrigerant to the shell and the shell to ambient air, and also includes the motor cooling effects of suction chamber refrigerant. In the current work, the suction chamber cooling of the motor has not been considered, but discharge chamber heat transfer to the shell has been accounted for.

1.3.2 Valve Models

Fixed-diameter orifices, capillary tubes, thermostatic expansion valves and electronic expansion valves are used in vapor compression systems to regulate refrigerant flow and provide the Joule-Thomson expansion process.

Li et al. (2004) developed physics-based models of adjustable throat area valves using manufacturer's data, examining three types of valve geometries. The models developed are strictly steady-state. Qiao (2014) developed a TXV model where the expansion process was treated as quasi-steady state, but a time constant was added to account for delay caused by the thermal resistance of the sensor bulb.

Hermes et al. (2010a and 2010b) developed models for adiabatic and non-adiabatic capillary tubes for small-scale refrigerator applications, and use in suction line heat exchangers respectively. In this work, only the adiabatic model has been developed.

1.3.3 Heat Exchanger Models

In general, three approaches are usually employed for modeling heat exchangers (Rasmussen, 2012a): lumped-parameter models, moving boundary models or discretized finite volume models. The details of these modeling methods are discussed next.

1.3.3.1 Lumped Parameter Model

For the purposes of this discussion, lumped parameter models are defined as those that consider the entire heat exchanger to be a single, stirred-tank control volume with single values for state variables like pressure and enthalpy. This is different to moving boundary models which divide the heat exchanger volume into a number of control volumes depending on the fluid phases present internally, and treat each phase as a lumped volume, although some authors (Rasmussen, 2012a) combine them into one category. Lumped parameter models are often employed in applications where the primary objective is control-oriented rather than accurate modeling of physical phenomenon (Qi and Deng, 2008). In studies where non-trivial lumped models are presented, either limited validations are presented (Chi and Didion, 1982) or only qualitative agreement is demonstrated (Sami et al., 1987), and higher order dynamics are generally not captured (Rasmussen, 2012a).

1.3.3.2 Moving Boundary Model

Moving boundary models divide the heat exchanger internal volume into a varying number of control volumes, with each control volume corresponding to a specific fluid phase. For evaporators, there are typically two control volumes for two-phase and vapor states whereas for condensers there is an additional control volume for liquid phase. The size of the control volume varies depending on the length of the fluid

phase. In addition, switching schemes are typically applied to handle the appearance or disappearance of states in startup/shutdown cases. To accurately account for the refrigerant mass inside the heat exchanger, these models typically apply mean void fraction correlations. Rasmussen (2012a) notes that, with one exception, all moving boundary formulations neglect the effects pressure drop in heat exchangers.

Moving boundary models are typically lower order models and are more suited for control applications where a compromise in accuracy for the sake of computational efficiency is justified. In addition, moving boundary models are also limited in their flexibility in handling different heat exchanger tube circuitries. Qiao (2014) describe the development of detailed moving boundary models with an adaptation to handle HX circuitry and provide experimental validation.

1.3.3.3 Discretized Models

A discretized heat exchanger model divides the heat exchanger volume into a finite number of control volumes of equal size and applies the discretized forms of conservations equations to them. The finite volume approach allows flexibility in handling more complicated refrigerant circuitries like multiple inlet tubes or multiple tube banks without the simplifying assumption of treating the heat exchanger as a single tube. In addition, air side dehumidification can be accounted for more easily due to the control volume nature of the model.

Traditionally, the models developed using the discretized scheme have considered thermodynamic properties to be averaged within a control volume, and have assumed homogeneous equilibrium flow for two-phase fluid (MacArthur, 1984). In such cases, refrigerant mass prediction is heavily dependent on the level of discretization. Some researchers account for different phase velocities for liquid and

vapor phase, but otherwise treat the two phases to be in equilibrium. Such assumptions are typically called Inhomogeneous flow (MacArthur and Grald, 1987). The most complex method is called the Separated Flow Model which accounts for the lack of thermodynamic equilibrium between the fluid phases. Qiao (2014) implements this method in the finite volume heat exchanger model developed.

Heat exchanger pressure drop is accounted for in a variety of ways. While some studies neglect pressure drop (Bendapudi and Braun, 2002), in some cases the pressure drop is assumed to be concentrated at the outlet and calculated using a steady-state equation. Another method is to have alternating series of control volumes with static pressure drop elements between them (Qiao, 2014, Winkler, 2009). The most sophisticated models consider the full momentum equation (Zhang et al., 2009). However, this method adds to the stiffness of the differential equations, making it more challenging for solvers to handle. Zhang et al. (2009) provide a review of the three ways of dealing with momentum equation and conclude that the static equation gets the job done in terms of evaluating pressure drop, but is computationally more efficient than the full dynamic equation.

The literature review shows that a wide range of modeling methodologies have been applied towards the dynamic simulations of vapor compression systems. Some of the methods have been selected for further investigation for the purposes of the current work, and implemented in the developed models. A need for thorough validation has been recognized with particular emphasis on considering higher order dynamics.

1.4 Research Objectives

A research gap has been identified in the development of a comprehensive, flexible framework for vapor compression system that has been thoroughly validated and can be used for the relative analysis of alternative low-GWP refrigerants as potential drop-in replacements. The framework is to be used for the evaluation of performance of a residential heat pump unit under ASHRAE test conditions. For the simulation, charge optimization studies will be carried out to determine optimum charge levels for the baseline and alternative refrigerants. In addition, steady-state and cyclic test performances will be evaluated in both heating and cooling modes. Comparison of alternative refrigerants under both steady-state and transient conditions is challenging since the models must be able to predict the steady-state values with adequate accuracy, but also faithfully predict the relative differences in performance between the baseline and the alternatives. Additionally, salient transient trends should be reproduced in the simulations, including pressure levels, discharge temperatures and capacity differences.

The primary objective of the research is to develop a modeling framework that can meet these challenges. With an eye towards usage beyond the current application, the framework is to be built on the widely-used platform Simulink® and is to include most of the commonly used components involved in heat pump systems. The components must all have unified boundary conditions so that arbitrary system configurations can be simulated.

1.5 Organization of Thesis

Chapter 2 discusses the overall framework structure, along with modeling details of individual components. In Chapter 3, the experimental facility is described along with details of the tested unit. Details about model implementation, along with model inputs are also described. The charge optimization studies are discussed, followed by combined heating and cooling steady-state test results. Lastly, the dynamic tests are discussed first for cooling mode and then for heating mode. Chapter 4 lists the conclusions of this work alongside future work. Key contributions of this thesis are also outlined.

2 Component Modeling

This chapter describes the overall structure of the framework developed for transient simulations of vapor compression systems and discusses modeling details of individual components.

The dynamics associated with vapor compression systems can be assumed to be dominated by the heat exchanger (Winkler, 2009). Therefore, the expansion and compression processes have been treated as quasi-steady-state phenomena in this work, although the dynamics of heat transfer through the compressor shell have been considered. The momentum equation has been decoupled from the mass and energy balance equations and an explicit, algebraic form of the equation has been applied to account for pressure drop in components.

The following component models have been developed and are discussed in subsequent sections of this chapter:

- Plain-fin, round-tube heat exchanger
- Efficiency-based scroll compressor
- Map-based generic compressor
- Scroll compressor with vapor injection port
- Generic, fixed diameter orifice
- Adiabatic capillary tube
- Thermostatic expansion valve
- Electronic expansion valve
- Reversing flow valve
- Connecting pipe

- Accumulator/Receiver
- Flash tank

The following sections describe the modeling approach used for the development of the framework, including the overall component structure, how reverse flows are handled and how the initial conditions are specified. This is followed by details of the individual component models.

2.1 Fluid Properties

Refrigerant property calculations are central to numerical analysis of vapor compression systems, and can often cause performance bottlenecks during transient simulations. Several researchers (Rasmussen, 2002, Tummescheit, 2002) use lookup tables for refrigerant properties, in order to reduce computation time, however there can be some numerical issues in calculating differential coefficients, since the interpolation between successive mesh points for the table are linear (Ding, 2007). The current framework is capable of handling several types of pure fluids and refrigerant mixtures, including user-defined mixtures. Fluid properties are evaluated using an enhancement of NIST's REFPROP 9.1 database (Lemmon et al., 2013) developed in-house. Details of the enhanced property call routines can be found in Aute and Radermacher (2014).

2.2 Component Structure

The overall goal in developing the framework is to allow the modeling and simulation of cycles with arbitrary component configurations. To accommodate this, all component models must have the same boundary conditions so that they may be connected in any order. Each component has been modeled containing two distinct

elements within it that each requires different boundary conditions (Tummescheit, 2002):

1. The first type are heat-transfer elements which require inlet and outlet mass flow rates and the inlet enthalpy as boundary conditions. Mass and energy balance equations are applied to these elements, and they calculate the inlet and outlet pressures and outlet enthalpy.
2. The second type are mass flow elements, or throttle elements, that require the inlet and outlet pressures and inlet enthalpy, and calculate the inlet and outlet mass flow rates and outlet enthalpy. These elements account for the quasi-steady momentum balance.

Each component consists of first a heat transfer element followed by a mass flow element. As a whole, each component requires the inlet mass flow rate and enthalpy as well as outlet pressure. It calculates the inlet pressure and the outlet mass flow rate and enthalpy. In this way, any component can be connected to any other component, and the boundary condition structure is maintained. A schematic of the component structure is shown in Figure 2.1. Note that the arrows do not represent refrigerant flow direction (which is from left to right) but only the flow of information through signals.

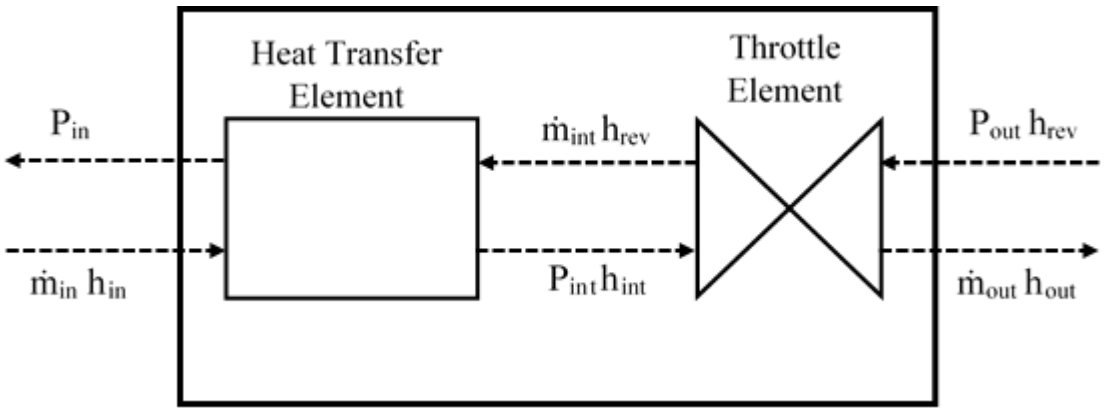

Figure 2.1. Component Structure

2.3 Upwind Scheme and Reverse Flows

During cycle startup or shutdown, it is possible that localized operating conditions within a component might cause refrigerant to flow in the reverse direction briefly. It is important to account for this phenomenon to ensure faithful reproduction of cycle transients. In fluid flow that is primarily convective, the upwind scheme is recommended for calculating thermodynamic properties, to avoid obtaining non-physical solutions (Patankar, 1980). Using central difference schemes to evaluate the properties can often lead to solutions where the parameter values at the *interfaces* are both greater or both lower than the value of the parameter inside the control volume (the Scarborough criterion is not satisfied and thus, convergence cannot be guaranteed).

In the current work, each component has inlet and outlet ports. At inlet ports, flow is considered positive if it is into the component. At outlet ports, flow is positive if it flows out of the component. This is a consequence of the causal modeling platform that is signal-based. By contrast, for acausal languages such as Modelica®, the convention of positive-flow-into-the-component is maintained for both inlet and outlet ports.

The boundary conditions during positive flow are inlet mass flow rate, inlet enthalpy and outlet pressure. In case of reverse flow, the enthalpy of the first element *upstream* of the *reversed* flow is used as the boundary condition, thus maintaining the upwind scheme. This can be seen in Figure 2.1 as the upstream propagated enthalpy h_{rev}. It is worthwhile to note that this reverse flow enthalpy, while always propagated upstream, is utilized only when there is reverse flow.

2.4 Initial Conditions Specification

One of the stated objectives of this work is to allow the components developed here be useful beyond the current work. It is essential that the input parameters to models be intuitive to use. One important consideration in this aspect is of the component initial conditions. The state variables used are the pressure and specific enthalpy of each control volume. Using specific enthalpy, as opposed to density or internal energy for example, has the advantage of always indicating whether the fluid is in single phase or two-phase.

Given the relative nature of specific enthalpy, however, it is not advisable to use enthalpy as an input when specifying initial conditions. Instead, the initial conditions are specified using one of the following methods:

- Single-phase pressure and temperature
- Saturation pressure and saturation ΔT (superheat/subcool value)
- Saturation temperature and saturation ΔT
- Saturation pressure and static vapor quality
- Saturation temperature and static vapor quality

The enthalpy value is then calculated using the inputs. These parameters cover the typical methods in which the initial conditions might be available to the engineer.

2.5 Heat Exchanger

2.5.1 Overview

Plain-fin, round-tube heat exchangers are commonly used in heat pump applications. Such heat exchangers have refrigerant flowing through the circular cross-section tubes and air passing over the extended surfaces, driven by a fan.

A schematic of the heat exchanger model is shown in Figure 2.2. The figure shows a sample heat exchanger with two banks of tubes, and three tubes in each bank. The tubes are assumed to be in series, with the outlet refrigerant from the first tube entering the second tube and so on. The outlet from the first bank enters the second bank of tubes. On the air side, the first bank of tubes is assumed have uniform air inlet temperature and humidity ratio, and air flow maldistribution is neglected. The air inlet temperature and humidity ratios for subsequent banks of tubes are calculated as outlets from previous banks. The figure does not show humidity ratios. The control volumes for the tube wall can also be seen, which account for the thermal mass from both the tube and the fins. Fin efficiency correlations, described later, are used to calculate the equivalent thermal masses.

A staggered grid scheme is used on the refrigerant side in solving the governing equations (Qiao, 2014). The mass and energy balance equations are solved for the control volumes, whereas the mass flow rates are evaluated for the interface between adjacent volumes. The input parameters required for the heat exchanger are listed in Table 2.1.

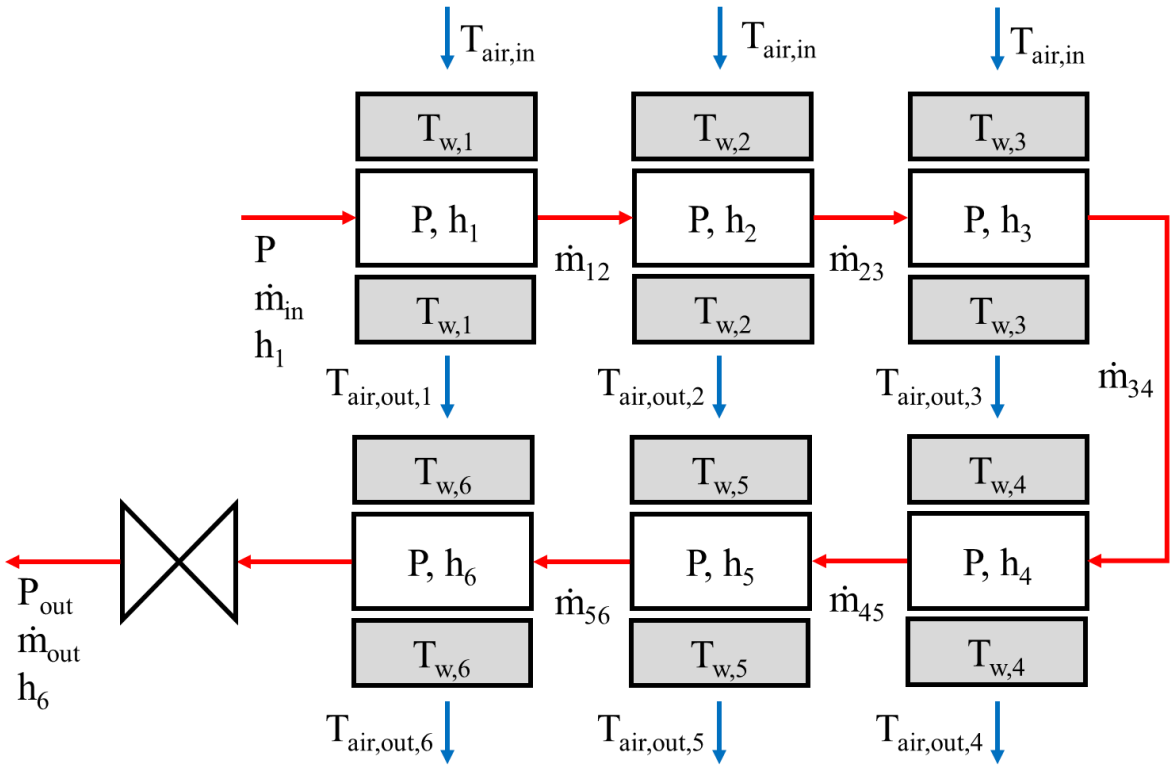

Figure 2.2. Heat Exchanger Schematic

Table 2.1. Heat Exchanger Input Parameters

Parameter	Units
TUBES	
Tube Configuration	Staggered or Inline
Number of Segments per Tube	-
Number of Tubes per Bank	-
Number of Banks of Tubes	-
Number of Parallel Coils	-
Tube Length	m
Tube Outer Diameter	m
Tube Thickness	m
Tube Vertical Spacing	m
Tube Horizontal Spacing	m
Tube Material	-
FINS	
Fin Type	Plate Fin With or Without Collar or Bare Tubes
Fins Per Meter	1/m
Fin Thickness	m
Fin Material	-
REFRIGERANT SIDE	
Vapor Phase Heat Transfer Coefficient	W
Two Phase Heat Transfer Coefficient	W/m^2K
Liquid Phase Heat Transfer Coefficient	W/m^2K
Nominal Mass Flow Rate	kg/s
Nominal Pressure Drop	Pa
AIR SIDE	
Heat Transfer Coefficient Correlation	-
State Parameters	RH *or* WBT
Inlet Dry Bulb Temperature	K
Inlet RH/Wet Bulb Temperature	% *or* K
Inlet Pressure	Pa
Air Flow	kg/s *or* m^3/s *or* m/s

2.5.2 Refrigerant-Side Modeling

The refrigerant flow inside the heat exchanger tubes is treated as one-dimensional, with properties considered uniform or averaged across the cross section. The following assumptions have been made in the governing equations of the heat exchanger:

1. Flow is one dimensional
2. Axial conduction is neglected
3. The refrigerant tube and fin are treated as having a constant temperature for a given control volume, with fin effects accounted for through fin efficiency calculations
4. Pressure drop in the heat exchanger is concentrated at the outlet of the last control volume. Thus, all control volumes themselves are at uniform pressure, yet the heat exchanger component still accounts for a pressure drop.

The governing partial differential equation of mass and energy conservation under the above assumptions are given below.

$$\frac{\partial \rho}{\partial t} + \frac{\partial (\rho v)}{\partial x} = 0 \tag{2.1}$$

$$\frac{\partial (\rho u V)}{\partial t} + \frac{\partial (\rho v h)}{\partial x} + \delta \dot{Q}_{ref} = 0 \tag{2.2}$$

For an individual, discretized control volume, the conservation equations can be rewritten as per equations (2.3) and (2.4).

$$\frac{\partial (\rho v)_i}{\partial t} + \dot{m}_i - \dot{m}_{i-1} = 0 \tag{2.3}$$

$$\frac{\partial (\rho u V)_i}{\partial t} + \dot{m}_{i-1} h_{i-1} - \dot{m}_i h_i + \delta \dot{Q}_{ref} = 0 \tag{2.4}$$

Traditionally, the transient simulation of vapor compression systems involves selection of two state variables, which can be used to derive all other thermodynamic properties associated with the component. In this work, pressure and specific enthalpy have been selected as the state variables. The density can thus be calculated as a function of these two variables in the form ρ = f (p, h). Using this, the partial derivative of density with respect to time can be calculated as a function of pressure and enthalpy using the chain rule, as shown in equation (2.5).

$$\frac{\partial \rho}{\partial t} = \left.\frac{\partial \rho}{\partial P}\right|_h \frac{dP}{dt} + \left.\frac{\partial \rho}{\partial h}\right|_P \frac{dh}{dt} \tag{2.5}$$

Thus, the discretized mass balance equation can be written as follows.

$$V_i \left[\left.\frac{\partial \rho}{\partial P}\right|_{h,i} \frac{dP}{dt} + \left.\frac{\partial \rho}{\partial h}\right|_{P,i} \frac{dh}{dt} \right] = \dot{m}_i - \dot{m}_{i-1} \tag{2.6}$$

Equation (2.7) shows the discretized energy balance equation.

$$V_i \left[\left(h_i \left.\frac{\partial \rho}{\partial P}\right|_{h,i} - 1 \right) \frac{dP}{dt} + \left(h_i \left.\frac{\partial \rho_i}{\partial h_i}\right|_{\mathrm{P},i} + \rho_i \right) \frac{dh_i}{dt} \right] = \dot{m}_{i-1} h_{i-1} - \dot{m}_i h_i - \dot{Q}_{ref,i} \tag{2.7}$$

The heat transfer between the refrigerant and tube wall is calculated as:

$$\dot{Q}_{ref} = \alpha . A_i . (T_w - T_r) \tag{2.8}$$

The heat transfer coefficient is input as a constant value for each of the three refrigerant phases (i.e., liquid, vapor and two-phase). In order to prevent abrupt changes in the heat transfer coefficient when the refrigerant undergoes a change of phase, a smoothing function is applied to the heat transfer coefficients in the threshold regions, that is, when vapor quality ranges from $0 < x < 0.2$ and $0.8 < x < 1$. Equation (2.9) shows the polynomial, with x_1 and x_2 being 0.2 and 0.8, respectively.

$$\alpha = \begin{cases} \alpha_l \qquad if\ x < 0 \\ \\ \dfrac{-2(\alpha_{tp} - \alpha_l)}{0.2^3} x^3 + \dfrac{3(\alpha_{tp} - \alpha_l)}{0.2^2} x^2 + \alpha_l \qquad if\ 0 \le x \le 0.2 \\ \\ \alpha_{tp} \qquad if\ 0.2 < x < 0.8 \\ \\ a = \dfrac{2(\alpha_v - a_{tp})}{(x_2 - 1)^3} x^3 - \dfrac{3(x_2 + 1)(a_v - a_{tp})}{(x_2 - 1)^3} x^2 + \left(\dfrac{-6(a_v - a_{tp})}{(x_2 - 1)^3} + \dfrac{6(x_2 + 1)(a_v - a_{tp})}{(x_2 - 1)^3} \right) x + \\ \left(a_v - \dfrac{2(a_v - a_{tp})}{(x_2 - 1)^3} + \dfrac{3(x_2 + 1)(a_v - a_{tp})}{(x_2 - 1)^3} + \dfrac{6(a_v - a_{tp})}{(x_2 - 1)^3} - \dfrac{6(x_2 + 1)(a_v - a_{tp})}{(x_2 - 1)^3} \right) \qquad if\ 0.8 \le x \le 1 \\ \\ \alpha_v \qquad if\ x > 1 \end{cases} \tag{2.9}$$

The resultant heat transfer coefficient is shown in Figure 2.3 for a hypothetical example.

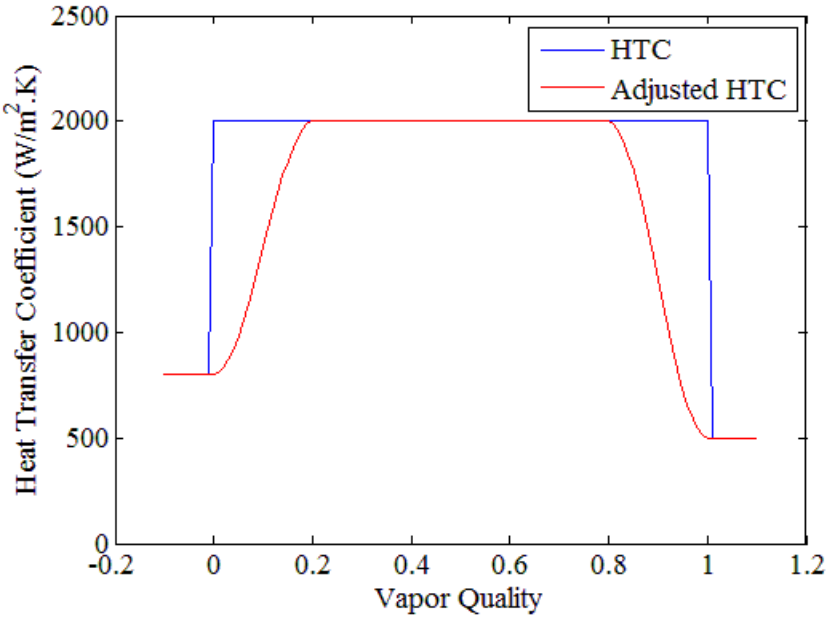

Figure 2.3. Adjusted Heat Transfer Coefficient

Finally, the heat transfer coefficients are assumed to have been calculated for a nominal mass flow rate $\dot{m}_0$. A correction term is applied to obtain the coefficient for the actual mass flow rate, as shown in equation (2.10) below.

$$\alpha_{actual} = \left(\frac{\dot{m}_{actual}}{\dot{m}_0} \right)^{0.8} \alpha_0 \tag{2.10}$$

Thus, a set of 2N differential algebraic equations are obtained where the state vector is given as follows:

$$\vec{y} = \left[\frac{dP}{dt}, \frac{dh_1}{dt}, \frac{dh_2}{dt}, \ldots, \frac{dh_N}{dt}, \dot{m}_1, \dot{m}_2, \ldots, \dot{m}_{N-1} \right]^T \tag{2.11}$$

Where, $\dot{m}_i$ is the mass flow rate at the interface of the i^{th} and $(i+1)^{th}$ control volume.

Pressure drop in the heat exchanger is accounted for by including a small throttle element at the outlet of the heat exchanger (Elmqvist, 2003). A nominal pressure drop value for a nominal mass flow rate is given as input to the model, and is used to

calculate the pressure drop for the actual mass flow rate, as shown in equation (2.12). The equation assumes turbulent refrigerant flow.

$$\dot{m} = \frac{\dot{m}_0}{\sqrt{dP_0}} \sqrt{|P - P_{out}|}.sign(P - P_{out}) \tag{2.12}$$

Where, $\dot{m}_0$ and dP_0 are the nominal parameters.

However, using this correlation for small pressure drop values leads to the function having infinite slope at the origin. To avoid numerical issues associated with this, the correlation is adjusted for small pressure drop values to have a finite derivative around zero mass flow rate. Below the threshold, the PCHIP function available in MATLAB® is used to calculate the mass flow rate, which provides a piecewise cubic hermite interpolating polynomial. The difference for small values is shown in Figure 2.4.

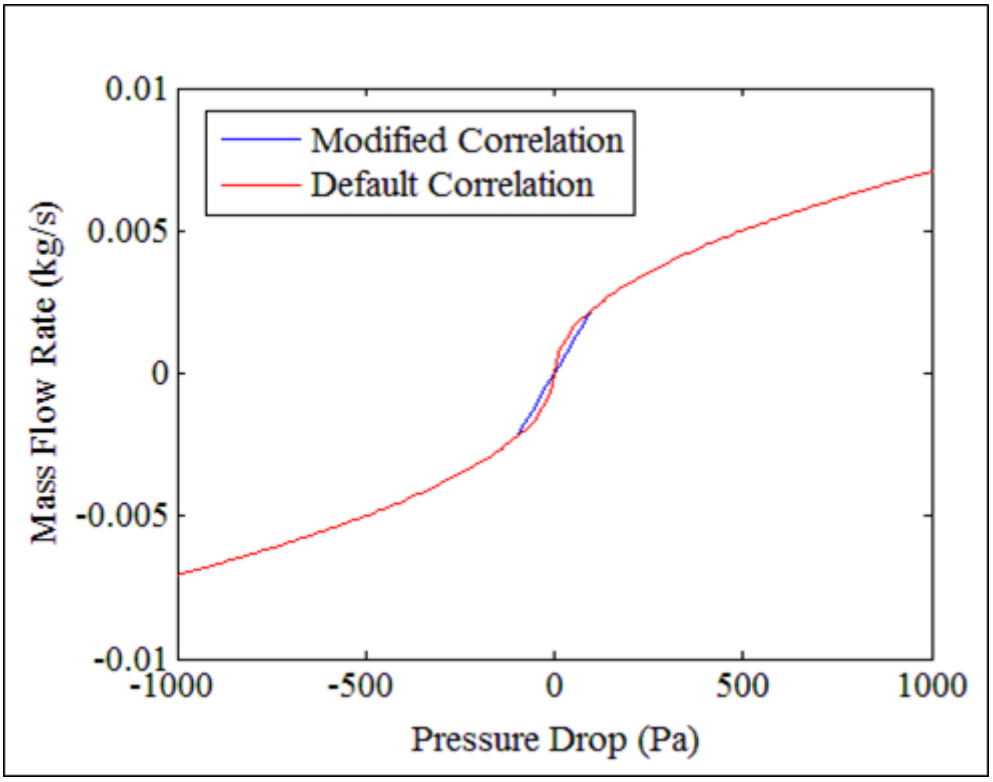

Figure 2.4. Pressure Drop Correlation Comparison

2.5.3 Tube Wall and Fin

An additional set of N equations are obtained by considering the energy balance on the heat exchanger wall. The difference in the rate of heat transfer between the refrigerant side and the air side leads to a change in temperature of the wall. This is calculated as shown in equation (2.13) below.

$$\frac{dT_{w,i}}{dt} = -\frac{(\dot{Q}_{ref,i} + \dot{Q}_{air,i})}{(M_{tube}c_{p,tube} + M_{fin}c_{p,fin})} \tag{2.13}$$

The refrigerant side heat transfer rate is calculated as per equation (2.8), whereas the air side is calculated using equation (2.29) or (2.30).

2.5.4 Air Flow Modeling

Fin tube heat exchangers are arranged in counterflow configuration. The flow on the air side is treated as one-dimensional. Heat and mass transfer is assumed to follow the Lewis analogy.

The air side geometric parameters are evaluated first. The equations for heat exchanger geometry are derived from Shah (2003). The primary and secondary air-side areas are calculated as shown in equations (2.14) and (2.15).

$$A_p = \pi D_c L(1 - f_{th}.\mathrm{FPM}) \times NTB \times NBT \tag{2.14}$$

$$A_s = 2\left(L_{HX}H_{HX} - \frac{\pi}{4}D_c^{\,2}.NTB.NBT\right)FPM.L + 2L_{HX}f_{th}FPM.L \tag{2.15}$$

Where, D_c is collar diameter, L is tube length, f_{th} is fin thickness, FPM is the number of fins per meter, NTB is number of tubes per bank and NBT is number of banks of

tubes, L_{HX} and H_{HX} are the heat exchanger length and height, respectively. The overall outer area, A_o, is the sum of primary and secondary areas.

The tubes can be arranged in either a staggered fashion or inline. The two types are shown in Figure 2.5 below, and can be specified as a model input.

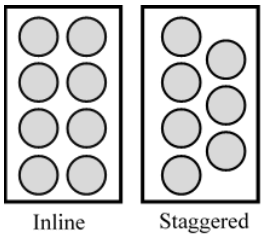

Figure 2.5. Inline and Staggered Tube Configurations

Depending on whether the tube configuration is inline or staggered, the minimum free flow area is calculated using equations (2.16) or (2.17), respectively.

$$A_{\min} = \frac{(P_t - D_c) L (1 - f_{th} FPM) H_{HX}}{P_t} \tag{2.16}$$

$$A_{\min} = \left(\frac{H_{HX}}{P_t} - 1 \right) z + (P_t - D_c)(1 - f_{th} FPM) L \tag{2.17}$$

where

$$z = \min(2x, 2y)$$

$$y = \left(\left(\frac{P_t}{2} \right)^2 + P_l^2 \right)^{0.5} - D_c - (P_t - D_c) f_{th} FPM$$

$$x = 0.5 * (P_t - D_c)(1 - f_{th} FPM)$$

Fin efficiency is calculated using the method presented in Hong and Webb (1996).

$$\eta_{fin} = \frac{\tanh(mr\phi)}{mr\phi} \cos(0.1 \times mr\phi) \tag{2.18}$$

$$m = \sqrt{\frac{2\alpha_0}{K_f f_{th}}} \tag{2.19}$$

$$r = \frac{D_o}{2} + f_{th} \tag{2.20}$$

$$\phi = \left(\frac{R_e}{r} - 1\right)\left(1 + 0.35\ln\left(\frac{R_e}{r}\right)\right) \tag{2.21}$$

Where, R_e is the radius of an equivalent circular fin with the same fin efficiency. It is calculated as shown below.

$$R_e = \frac{1.28 \times r \times P_t}{D_o + 2f_{th}}\left(\frac{P_l}{P_t} - 0.2\right)^{0.5} \tag{2.22}$$

The effective outer area is then found using equation (2.23).

$$A_{o,eff} = A_o + \eta_{fin} A_s \tag{2.23}$$

For the air side flow, air pressure drop is not considered, and fan work is thus neglected. Two operating modes are considered, fan-on (forced convection) and fan-off (natural convection). For the fan-on mode, the heat and mass transfer governing equations are given as follows:

$$\dot{m}_a c_{p,a} \frac{dT_a}{dy}\Delta y = \alpha_a A_{o,eff}(T_w - T_a) \tag{2.24}$$

$$\dot{m}_a \frac{d\omega_a}{dy}\Delta y = \alpha_m A_{o,eff} \min(0, \omega_{w,s} - \omega_a) \tag{2.25}$$

$\omega_{w,s}$ is the saturation humidity ratio at the wall surface temperature T_w and α_m is the mass transfer coefficient found using equation (2.26).

$$\alpha_m = \frac{\alpha_a}{c_{p,a} Le^{2/3}} \tag{2.26}$$

With $Le^{2/3}$ taken to be 0.9 (Kuehn et al., 1998).

Equations (2.24) and (2.25) can be solved to get the air outlet temperature and humidity ratio as per equation (2.27) and (2.28) below.

$$T_{a,out} = T_w - \left(T_w - T_{a,in}\right)\exp\left(\frac{-\alpha_a A_{o,eff}}{\left(\dot{m}_a / NTB\right)c_{p,a}}\right) \tag{2.27}$$

$$\omega_{a,\text{out}} = \omega_{a,in} + \left[1 - \exp\left(-\frac{\alpha_a A_{o,eff}}{\left(\dot{m}_a / NTB\right)c_{p,a} Le^{2/3}}\right)\right]\min(0, \omega_{a,s} - \omega_{a,in}) \tag{2.28}$$

The air side heat transfer is calculated as a sum of the sensible and latent heat loads and is given by equation (2.29).

$$\dot{Q}_a = \dot{m}_a c_{p,a}(T_{a,in} - T_{a,out}) + \dot{m}_a \Delta h_{fg}(\omega_{a,in} - \omega_{a,out}) \tag{2.29}$$

Where, Δh_{fg} is the enthalpy of vaporization of water and $c_{p,a}$ is the specific heat of moist air. The heat transfer coefficients, α_a, for fin tube heat exchangers is calculated using the correlation derived by Wang et al. (2000).

During fan-off conditions, heat exchange at the heat exchanger surface is assumed to be purely through natural convection, with a constant heat transfer coefficient and no condensation of moisture on the heat exchanger surface. The heat transfer on the air side is calculated as shown in equation (2.30) below.

$$\dot{Q}_a = \alpha_a A_{o,eff}(T_w - T_a) \tag{2.30}$$

2.6 Solving System of Equations

For a heat exchanger divided into N control volumes, a set of 3N DAEs are obtained, 2N for mass and energy balances, and N equations for HX wall energy balance. These DAEs can be written in matrix form as follows:

$$M(\vec{y}).\vec{y}' = \boldsymbol{f}(\vec{y}) \tag{2.31}$$

Where, M is a state-dependent, singular mass matrix and **f** is a function of the state variables.

Such a system of DAEs can be solved in Simulink® only if it is written in the semi-explicit form given in equations (2.32) and (2.33) (Shampine et al., 1999).

$$\boldsymbol{u}' = f_1(t, \boldsymbol{u}, \boldsymbol{v}) \tag{2.32}$$

$$0 = f_2(t, \boldsymbol{u}, \boldsymbol{v}) \tag{2.33}$$

Where,

u is the vector of differential variables, i.e. $[dP/dt,\ dh_1/dt, \ldots,\ dh_N/dt\ dTw_1/dt\ , \ldots,\ dTw_N/dt]^T$ and,

v is the vector of algebraic variables, i.e., $[\dot{m}_2, \dot{m}_3, \ldots, \dot{m}_N]^T$

The system of algebraic variables must thus be solved first and then fed into the ordinary differential equations as algebraic constraints on the solution. This leads to an algebraic loop being created where the function block calculates the values of the algebraic variables, but also requires these values as inputs. This problem is solved by inserting a single-time-step delay between the input and output of the block. For the first time step, this means that an initial value of the algebraic variables must also be specified in addition to the initial values of state variables that appear in their derivative form. This numerical issue does not appear in acausal modeling paradigms since they utilize methods that symbolically manipulate the constituent equations to determine the inter-dependencies of variables.

2.7 Compressor Models

Compressor models for transient simulations typically fall into three categories (Qiao, 2014): 1) Efficiency-based models, 2) Map-based models, and 3) Detailed models.

Compressor models are treated as quasi-steady state components in the current work since the timescales associated with the variation of compressor mass flow rate are very small compared to those associated with heat exchanger transients and refrigerant mass distribution (Winkler, 2009). However, a purely quasi-steady state model cannot capture the transients associated with thermal storage of the compressor shell, or the refrigerant storage inside the compressor volume. This will lead to inaccuracies in comparison of discharge temperature, which is an important consideration when evaluating drop-in refrigerants.

To resolve this issue, as well as to maintain the boundary condition requirements, the compressor models are developed with a small control volume that accounts for the transient phenomenon followed by a steady-state part which computes the compressor mass flow rate and power consumption. This method is derived from the work of Ding et al. (2007).

Three compressor models are available in the component library:

1. Generic, efficiency-based compressor
2. ARI 10-coefficient polynomial based compressor
3. Scroll compressor with vapor injection port

Table 2.2 gives the input parameters required for each of the models developed.

Table 2.2. Compressor Input Parameters

Parameter	Units	Parameter	Units
EFFICIENCY BASED COMPRESSOR		**VAPOR INJECTION SCROLL COMPRESSOR**	
Displacement	m^3/rev	Suction Chamber Volume	m^3
Shell Outer Diameter	m	Suction Chamber Volume	m^3
Shell Thickness	m	Economizer Port Volume	m^3
Shell Height	m	Discharge Chamber Volume	m^3
Shell Material	-	Displacement	m^3/rev
RPM	rev/min	RPM	rev/min
Isentropic Efficiency	-	Motor Efficiency	-
Volumetric Efficiency	-	Mechanical Efficiency	-
Motor Efficiency	-	Polytropic Index	-
Refrigerant-to-Shell Heat Transfer Coefficient	W/m^2K	First Stage Volume Ratio	-
Air-to-Shell Heat Transfer Coefficient	W/m^2K	Mass Flow Curve Fit Coefficients	-
Nominal Mass Flow Rate	kg/s	Power Curve Fit Coefficients	-
Nominal Pressure Drop	Pa	Refrigerant-to-Shell Heat Transfer Coefficient	W/m^2K
MAP-BASED COMPRESSOR		Air-to-Shell Heat Transfer Coefficient	W/m^2K
Volume	m^3	Nominal Mass Flow Rate	kg/s
RPM	rev/min	Nominal Pressure Drop	Pa
Map Coefficients	-		

2.7.1 Efficiency-Based Scroll Compressor

The generic scroll compressor model consists of three regions: the suction chamber, the scroll set and the discharge chamber. Typically, manufacturers do not provide many physical parameters related to the compressor internal structure, therefore, an effort has been made to only use generally available information to the extent possible. Specifically, internal free volume is often available for compressors. This volume is provided as a model input, and an assumption is made that 80% of the free volume is in the suction chamber, whereas 20% is in the discharge chamber.

2.7.1.1 Suction Chamber

The suction chamber is modeled as an adiabatic lumped volume with stirred-tank approximation and motor cooling has been neglected. Discretized mass and energy balance equations are applied to the chamber, as shown in equations (2.34) and (2.35).

$$V\frac{d\rho}{dt} = \dot{m}_{suc} - \dot{m}_1 \tag{2.34}$$

$$V\left(\rho\ \frac{dh}{dt} - \frac{dP}{dt}\right) = \dot{m}_{suc}(h_{suc} - h_1) \tag{2.35}$$

Here, point 1 is the outlet of the suction chamber (inlet of the scroll set).

2.7.1.2 Scroll Set

The compression process is modeled as quasi-steady state. The scroll compressor model requires the isentropic, volumetric and motor efficiencies to be provided as inputs.

The mass flow rate through the compressor is calculated as shown in equation (2.36) below.

$$\dot{m} = \eta_{vol}\rho_{in}D\frac{RPM}{60} \tag{2.36}$$

The outlet enthalpy from the compressor as well as the compressor power consumption are calculated as follows:

$$h_{out} = h_{in} + \frac{h_{out,s} - h_{in}}{\eta_{isen}} \tag{2.37}$$

$$\dot{W}_{comp} = \frac{\dot{m}(h_{out} - h_{in})}{\eta_{motor}} \tag{2.38}$$

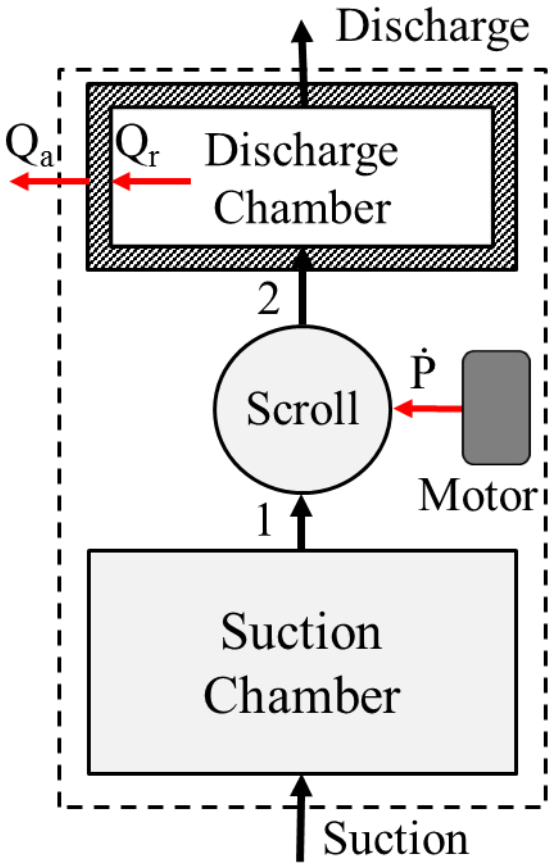

Figure 2.6. Scroll Compressor Schematic

2.7.1.3 Discharge Chamber

Upon compression, the refrigerant enters the discharge chamber. The total compressor weight is often available from manufacturers, and 20% of the weight is assumed to be the thermal mass of the discharge chamber. A lumped approach is also used here, with the mass and energy balance equations being derived in a similar manner to (2.34) and (2.35). The heat transfer from the refrigerant to the wall is calculated using equation (2.8). On the air side, the heat transfer is through natural convection only, as per equation (2.30).

At the outlet of the discharge chamber volume, a small mass flow element is modeled that provides a small pressure drop, in order to maintain the boundary condition structure.

2.7.2 Map-Based Compressor

ARI/AHRI establishes a method for evaluation of performance parameters for single and variable capacity positive displacement compressors (ARI Standard 540, 2004). It outlines a third-degree polynomial equation with ten coefficients to calculate refrigerant mass flow rate, power input, current and the compressor efficiency. The format of the polynomial equation is shown in equation (2.39).

$$X = C_1 + C_2.T_S + C_3.T_D + C_4.T_S^{\,2} + C_5.T_S.T_D + C_6.T_D^{\,2} + C_7.T_S^{\,3} + C_8.T_D.T_S^{\,2} + C_9.T_S.T_D^{\,2} + C_{10}.T_D^{\,3} \quad (2.39)$$

Where, X is compressor mass flow rate or compressor power consumption, C_1, C_2 ... C_{10} are the associated curve fit coefficients for the parameter under consideration, and T_S and T_D are the suction and discharge dew point temperatures respectively

The coefficients are provided by the manufacturer and input into the model. They are evaluated at standardized suction superheat values and correction terms must be applied to obtain the compressor parameters at the operating superheat. The correction for the superheat is calculated as per equation (2.40).

$$\dot{m}_{actual} = \frac{v_{map}}{v_{actual}} \dot{m}_{map} \quad (2.40)$$

Where, v is the specific volume for the relevant condition.

The limitation associated with this model is that it is suitable only for the operating range for which the coefficients have been derived. Thus, it does not lend itself well for extrapolative use, which is often necessary when startup and shutdown conditions are being simulated.

2.7.3 Scroll Compressor with Vapor-Injection Port

Vapor injection scroll compressors contain an economizer port through which vapor is injected into the scroll set to mix with the refrigerant inside. Refrigerant enters the compressor chamber on the suction side and is sucked into the scroll set. At the intermediate point, the compressed refrigerant is mixed with the injected vapor via the economizer port. The mixed vapor is then further compressed before being discharged through the discharge port.

The current model is based on the model developed by Qiao (2014). The following assumptions are made about the model:

1. Oil effects are neglected
2. Low and high stage compression processes have the same polytropic index

This compressor has two inlet ports and one outlet port. The boundary conditions for both inlet ports are the mass flow rate and enthalpy, whereas for the discharge (outlet) port are the outlet pressure. To accommodate the boundary conditions, at the economizer port, a small control volume is included whereas at the discharge port, a small throttle element is included.

2.7.3.1 Suction Chamber

The mass and energy conservation equations are applied to the suction chamber. These equations are shown below in equations (2.41) and (2.42).

$$V_1 \frac{d\rho_1}{dt} = \dot{m}_{suc} - \dot{m}_1 \tag{2.41}$$

$$V_1 \left(\rho_1 \frac{dh_1}{dt} - \frac{dP_1}{dt} \right) = \dot{m}_{suc} (h_{suc} - h_1) \tag{2.42}$$

These equations are applied in their discretized form with the partial derivative of density represented as a function of state variables pressure and enthalpy. The mass flow rate at the suction of the scroll set is determined using a curve fit, as shown in equation (2.43).

$$\dot{m}_{suc} = \left(a_1 - a_2 \left(\frac{P_{dis}}{P_{suc}} \right)^{1/n} \right) \rho_{suc} V_{disp} \frac{RPM}{60} \tag{2.43}$$

Where n is the polytropic index and a_1 and a_2 are curve fit coefficients. Flow through the economizer port is calculated in an analogous manner to flow through a fixed orifice.

$$\dot{m}_{econ} = sign(p_{inj} - p_{\text{int}}) a_3 \sqrt{\rho} \tag{2.44}$$

Where p_{inj} is the injection pressure and p_{int} is the intermediate pressure. If the intermediate pressure is higher than the injection pressure, vapor is forced out of the compressor through the injection port, leading to a reverse flow. The enthalpy after the mixing process is calculated as :

$$h_{mix} = \begin{cases} \dfrac{\dot{m}_{suc} h_{\text{int}} + \dot{m}_2 h_2}{\dot{m}_1 + \dot{m}_2} & when\ p_2 - p_{\text{int}} > 0 \\ h_{\text{int}} & when\ p_2 - p_{\text{int}} \le 0 \end{cases} \tag{2.45}$$

The discharge mass flow rate is calculated as per equation (2.46).

$$\dot{m}_{dis} = \frac{\sqrt{\rho_4 (P_4 - P_{dis})}}{f_{dis}} \tag{2.46}$$

Finally, the compressor work is calculated using the curve fit equation derived by Qiao (2014).

$$\dot{W}_{comp} = b_1 P_{suc} \dot{V}_1 \left(\left(\frac{P_{\text{int}}}{P_1} \right)^{b_2} - 1 \right) + b_3 P_{\text{int}} \dot{V}_{mix} \left(\left(\frac{P_4}{P_{\text{int}}} \right)^{b_4} - 1 \right) + b_5 \tag{2.47}$$

The scroll compressor schematic is shown in Figure 2.7 below

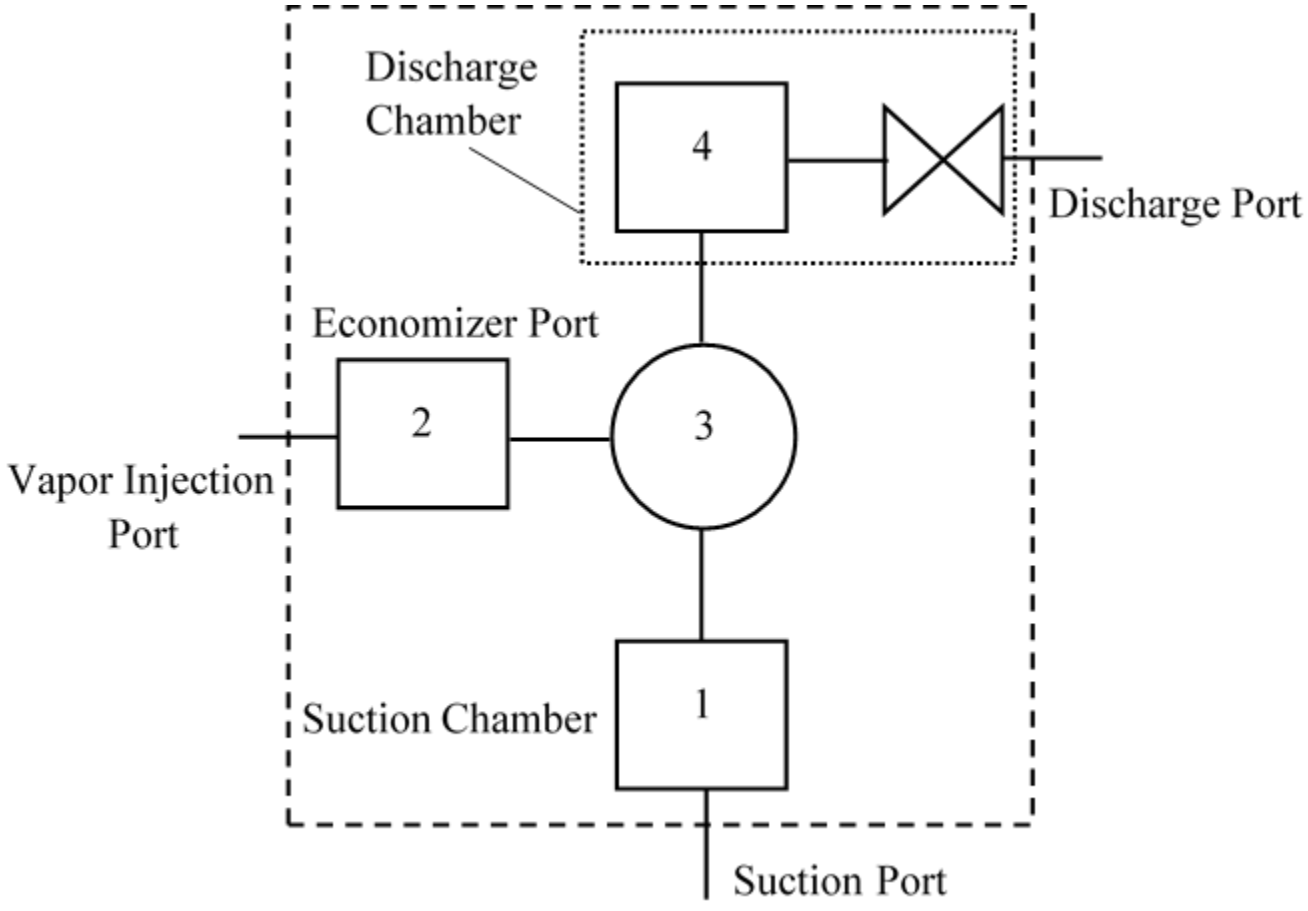

Figure 2.7. Vapor Injection Scroll Compressor Schematic

2.8 Valve Models

Valves serve a variety of purposes in vapor compression systems. They are used for isenthalpic expansion of refrigerants to low pressures, controlling the superheat of the refrigerant entering the compressor, controlling flow direction of the refrigerant, and as release valves. The following valve models have been developed in the current work:

- Generic, fixed-diameter orifice
- Adiabatic capillary tube
- Thermostatic expansion valve
- Electronic expansion valve
- Reversing valve

The valve models, like the compressor models, consist of a small control volume at the inlet followed by throttle element. The expansion process is treated as a quasi-steady state process for similar reasons as the compressor models. Table 2.3 shows the list of input parameters required for the different valve types.

2.8.1 Fixed-Diameter Orifice

The fixed diameter orifice is an expansion device with no active controls. The expansion process is assumed to be isenthalpic. The mass flow rate through the valve is calculated using equation (2.48).

$$\dot{m} = C_v . \phi_i^2 . \sqrt{\rho . (p_{in} - p_{out})} \tag{2.48}$$

Where, C_v is the flow coefficient of the valve, available as manufacturer data, and provided as an input to the model.

Table 2.3. Valve Input Parameters

Parameter	Units	Parameter	Units
FIXED DIAMETER ORIFICE		**THERMOSTATIC EXPANSION VALVE**	
Volume	m^3	Volume	m^3
Orifice Diameter	m	Orifice Diameter	m
Flow Coefficient	-	Rod (Stem) Diameter	m
ADIABATIC CAPILLARY TUBE		Pin Diameter	m
Volume	m^3	Pin Height	m
Outer Diameter	m	Minimum Opening Area	m^2
Thickness	m	Flow Coefficient	-
Length	m	Valve Time Constant	s
ELECTRONIC EXPANSION VALVE		Initial Spring Force	N/m^2
Volume	m^3	G-Factor	N/m^3
Orifice Diameter	m	**REVERSING VALVE**	
Flow Coefficient	-	Volume	m^3
Superheat Setpoint	K	Time Constant	s
Curve-fit Coefficients	-	Minimum Opening	-

2.8.2 Adiabatic Capillary Tube

Capillary tube models are simple, small diameter pipes that are often used in small-capacity (under 5 kW) refrigeration applications. The model for the tube is based on the work of Hermes et al. (2010a). The model finds an explicit solution for the mass flow rate and is semi-empirical in nature. The following assumptions are made in the derivation of the model:

1. Flow is isenthalpic through the valve
2. Pressure drop due to acceleration of flow is much smaller compared to frictional pressure drop

The mass flow rate is calculated using equation (2.49) shown below.

$$\dot{m} = \left\{ \frac{\pi^{2-d} 2^{2d-3}}{c} \frac{D^{5-d}}{\mu_f L} \left[\frac{p_c - p_f}{v_f} + \frac{p_f - p_e}{a} + \frac{b}{a^2} \ln\left(\frac{a p_e + b}{a p_f + b} \right) \right] \right\}^{\frac{1}{2-d}} \quad (2.49)$$

Here, D is the diameter of the tube,

L is capillary tube length,

p_f is the flash point pressure which is calculated iteratively using Newton's method,

p_c and p_e are the condensing and evaporating pressures respectively,

c and d are constants that have the value of 0.14 and 0.15 respectively, and,

a and b are parameters that are calculated using equations (2.50) and (2.51) respectively.

$$a = v_f(1-k) \tag{2.50}$$

$$b = v_f . p_f . k \tag{2.51}$$

With, $k = 1.63\times10^5 \, p_f^{\,-0.72}$

2.8.3 Thermostatic Expansion Valve

Thermostatic expansion valves (TXV) consist of a sensor bulb attached to the suction line that is filled with refrigerant. The refrigerant within the bulb exerts a pressure on a diaphragm inside the TXV through the means of a capillary tube. The resultant force acting on the diaphragm determines the spring deflection. In turn, this deflection is correlated to the valve opening area by considering the geometry of the valve. A schematic of the TXV is shown in Figure 2.8. The model developed by Qiao (2014) is used as a reference for this model.

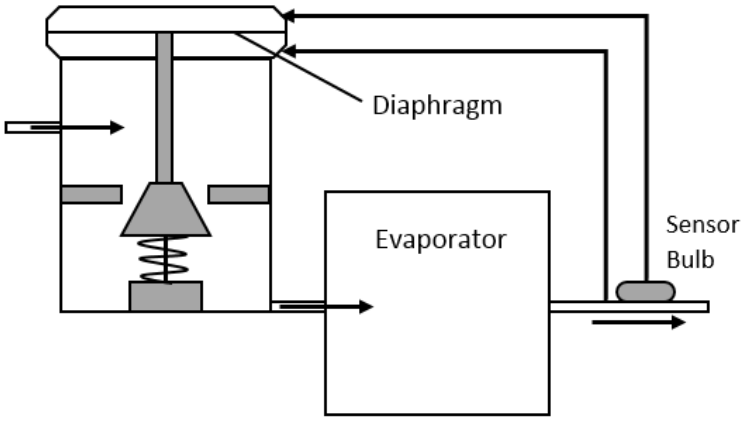

Figure 2.8. Thermostatic Expansion Valve

As the bulb senses an increase or decrease in the superheat, it affects the force balance on the diaphragm, causing the valve to open further or close more. This subsequently increases or decreases the mass flow rate through the evaporator, and acts to correct the outlet superheat. Due to the thermal resistance of the sensor bulb, there is a delay in the change of the bulb temperature. This is accounted for using a first order time constant calculated as shown in equation (2.52).

$$\frac{dT_b}{dt} = \frac{T_{ref} - T_b}{\tau_b} \tag{2.52}$$

To calculate the spring deflection, the force balance on the diaphragm is evaluated as per equation (2.53).

$$\kappa y + F_{offset} = (p_b - p_{eq})\mathrm{A}_{diaphragm} \tag{2.53}$$

Here, K is the spring constant, y is the deflection, p_b is the vapor pressure in the bulb, p_{eq} is the equalization pressure that acts to close the valve and F_{offset} is the force exerted through the initial deflection of the spring. The maximum flow area possible through the valve is given as

$$A_{\max} = \frac{\pi}{4}\left(d_{orif}^2 - d_{rod}^2\right) \tag{2.54}$$

The horizontal opening area is found using equation (2.55).

$$A_{hor} = \frac{\pi}{4} d_{orif}^2 - \pi\left(\frac{d_{rod}}{2} + \max(0, y_0 - y)\right)\left(\frac{d_{pin} - d_{rod}}{2H_{pin}}\right)^2 \tag{2.55}$$

Here, y is the deflection of the diaphragm and y_0 is the deflection of the pin calculated using equations (2.56) and (2.57).

$$y = \frac{p_{bulb} - p_{in} - offset}{G} \tag{2.56}$$

$$y_0 = \frac{d_{orif} - d_{rod}}{d_{pin} - d_{rod}} H_{pin} \tag{2.57}$$

Where, d_{orif} is the diameter of the valve opening and d_{rod} is the maximum diameter of the closing portion of the valve and d_{pin} is the valve stem diameter. The effective open area is then calculated as:

$$A_{eff} = \max(A_{\min}, \min(A_{\max}, A_{hor})) \tag{2.58}$$

2.8.4 Electronic Expansion Valve

Electronic expansion valves (EEVs) typically include a pressure sensor and an in-stream thermocouple on the vapor line to calculate the superheat. The EEV controller determines this superheat and then controls the valve opening to bring it to the setpoint.

For an EEV, it is harder to establish a relation between the flow area and valve opening. Instead, the combined value of $C_v.A$ is evaluated by applying regression on experimental data.

$$C_v A = c_0 + c_1\varphi + c_2\varphi^2 + c_3\varphi^3 \tag{2.59}$$

Where, φ is the percentage of valve opening, and is determined through a PI controller that uses the error between measured superheat and the setpoint (equation (2.60)).

$$\varphi(t) = K_p e(t) + K_i \int_0^t e(\tau) d\tau \tag{2.60}$$

The mass flow rate is then calculated using equation (2.61).

$$\dot{m} = C_v A \sqrt{\rho(p_{in} - p_{out})} \tag{2.61}$$

2.8.5 Reversing Flow Valve

Reversing valves are employed to enable switching of heat pumps between heating and cooling mode. The model developed by Qiao (2014) has been used as a basis for development. It consists of two small, adiabatic control volumes that are connected to four on/off valves as shown in Figure 2.9.

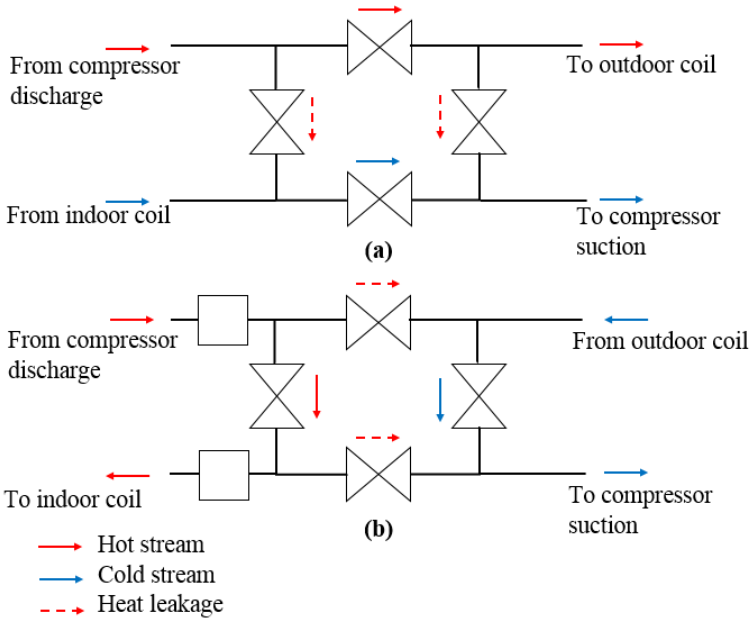

Figure 2.9. Reversing Flow Valve Schematic a) Cooling Mode b) Heating Mode

Flow is through one of two pairs of throttles, with the other pair considered to be in minimum opening position. Discretized mass and energy balance equations are applied to the control volumes. The mass flow rate through the throttle elements is calculated using equation (2.62) below.

$$\dot{m} = \varphi \frac{\sqrt{\rho_{in} \Delta P}}{f} \tag{2.62}$$

Where, φ is the current valve opening (100% for fully open and 0.01% for closed valve) To calculate the heat leak between the hot and cold streams, a constant value for the thermal resistance, R_{rev}, is assumed and used in equation (2.63).

$$\dot{Q}_{rev} = \frac{T_{hot} - T_{cold}}{R_{rev}} \tag{2.63}$$

The switching between heating and cooling mode is not assumed to happen instantaneously. Instead, the transition period is accounted for as follows:

$$\frac{d\varphi}{dt} = \frac{1}{\tau}(\varphi_{target} - \varphi) \tag{2.64}$$

This model has the advantage that the two control volumes always have a throttle between them, thus maintaining the boundary conditions.

2.9 Other Components

Heat pump systems frequently include other component models such as pipes, accumulator/receivers or flash tanks. These models have also been developed and are described here. The input parameters for these models are summarized in Table 2.4 and Table 2.5.

Table 2.4. Pipe Input Parameters

Parameter	Units
Number of segments	-
Length	m
Outer Diameter	m
Thickness	m
Pipe Material	-
Refrigerant-to-Tube Heat Transfer Coefficient	W/m^2K
Air-to-Tube Heat Transfer Coefficient	W/m^2K
Nominal Mass Flow Rate	kg/s
Nominal Pressure Drop	Pa
Ambient Air Temperature	K

2.9.1 Pipe Model

The pipe model is developed in an analogous manner to the heat exchanger model, with discretized mass and energy balance equations applied to the finite, equal sized control volumes. The model differs from the heat exchanger model in the following ways:

- The pipe is always a single bank of control volumes placed in series
- Heat transfer on the air side is through natural convection only, with the heat transfer coefficient provided as an input.

Table 2.5. Accumulator and Flash Tank Input Parameters

Parameter	Units	Parameter	Units
ACCUMULATOR		**FLASH TANK**	
Shell Height	m	Shell Height	m
Shell Inner Diameter	m	Shell Inner Diameter	m
Shell Thickness	m	Shell Thickness	m
Inlet Pipe Inner Diameter	m	Inlet Pipe Inner Diameter	m
Outlet Pipe Inner Diameter	m	Vapor Pipe Inlet Diameter	m
Inlet Pipe Height	m	Liquid Pipe Inner Diameter	m
Outlet Pipe Height	m	Inlet Pipe Height	m
Shell Material	-	Vapor Pipe Height	m
Refrigerant-to-Shell Heat Transfer Coefficient	W/m^2K	Liquid Pipe Height	m
Air-to-Shell Heat Transfer Coefficient	W/m^2K	Shell Material	-
Refrigerant Nominal Mass Flor Rate	kg/s	Refrigerant-to-Shell Heat Transfer Coefficient	W/m^2K
Refrigerant Nominal Pressure Drop	Pa	Air-to-Shell Heat Transfer Coefficient	W/m^2K
Ambient Air Temperature	K	Nominal Mass Flow Rate	kg/s
		Nominal Pressure Drop	Pa

2.9.2 Accumulator Model

Accumulators/Receivers are pressure vessels that serve as storage for excess refrigerant mass and also ensure that only pure vapor enters the compressor (in the case of accumulator) or that only saturated liquid enters the expansion device (in the case of receiver). They are modeled as a lumped control volume with averaged thermodynamic properties. The following assumptions are used to simplify the model:

1. Phase separation is considered ideal
2. Vapor and liquid phases in the flash tank are in thermodynamic equilibrium

Mass and energy balance equations are applied to the control volume as shown in equations (2.65) and (2.66).

$$V\frac{d\bar{\rho}}{dt} = \dot{m}_{in} - \dot{m}_{out} \tag{2.65}$$

$$V\left(h\left.\frac{\partial\rho}{\partial P}\right|_h - 1\right)\frac{dP}{dt} + V\left(h\left.\frac{\partial\rho}{\partial h}\right|_P + \rho\right)\frac{dh}{dt} = \dot{m}_{in}h_{in} - \dot{m}_{out}h_{out} + Q_r \qquad (2.66)$$

Density is again expressed as a function of pressure and specific enthalpy when calculating the derivatives. As in the pipe model, heat transfer on the air side is through natural convection. The difference in heat transfer rate between the air and refrigerant leads to a change in the shell temperature, determined as per equation (2.67).

$$\frac{dT_w}{dt} = \frac{-(Q_r + Q_a)}{C_{shell}} \qquad (2.67)$$

Where, C_{shell} is the thermal capacity of the accumulator shell.

The outlet enthalpy of the refrigerant leaving the accumulator is determined as follows:

$$h_{out} = \begin{cases} h_f & if\ H_{liq} > H_{out} + d_{out}\ (fully\ submerged) \\ h_g - \left(\frac{H_{liq} - H_{out}}{d_{out}}\right)\left(h_g - h_f\right) & if\ H_{out} + d_{out} \geq H_{liq} \geq H_{out}\ (partially\ submerged) \\ h_g & if\ H_{liq} < H_{out}\ (unsubmerged) \end{cases} \qquad (2.68)$$

Where, the height of the liquid is calculated using the following equation:

$$H_{liq} = \frac{\bar{\rho} - \rho_g}{\rho_f - \rho_g} H_{acc} \qquad (2.69)$$

A schematic of the accumulator with the various parameters is shown in Figure 2.10 below.

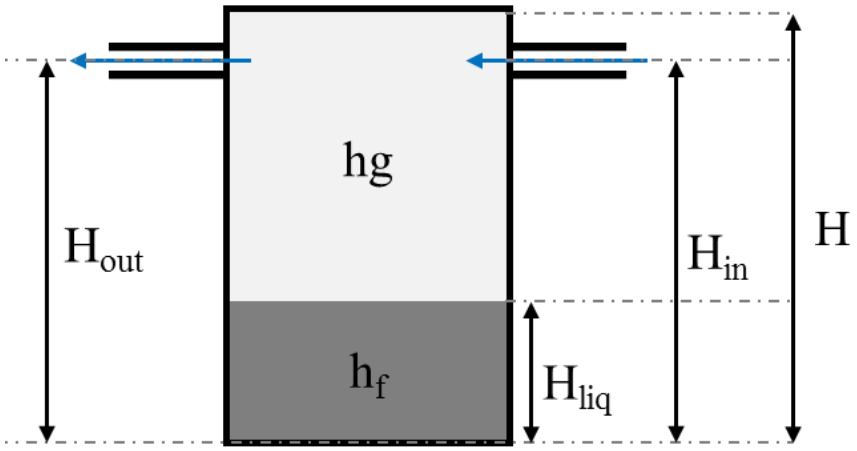

Figure 2.10. Accumulator Schematic

2.9.3 Flash Tank Model

Flash tanks are used in vapor compression systems to separate the fluid phases. The vapor phase is injected into the compressor through the vapor injection port whereas the liquid phase is fed into the expansion valve. The model in the current work is based on the model developed by Qiao (2014). The assumptions involved in the model are similar to those of the accumulator model, however, flash tanks have two outlet ports, and the outlet states of the refrigerant must be determined for each of those ports.

If the refrigerant inside the tank is in single phase, the enthalpies of both outlet ports is the mean enthalpy of the refrigerant inside the tank. If the refrigerant is in two phase, equation (2.70) is used to determine the outlet enthalpies, which is analogous to the equation (2.68) for the accumulator. Equation (2.69) is used to find the height of the liquid level.

$$h_{l,out} = \begin{cases} h_f & if\ H_{liq} > H_{l,out} + d_{l,out}\ (fully\ submerged) \\ h_g - \left(\dfrac{H_{liq} - H_{l,out}}{d_{l,out}} \right) \left(h_g - h_f \right) & if\ H_{l,out} + d_{l,out} \geq H_{liq} \geq H_{l,out}\ (partially\ submerged) \\ h_g & if\ H_{liq} < H_{l,out}\ (unsubmerged) \end{cases}$$

$$h_{\mathrm{v},out} = \begin{cases} h_f & if\ H_{liq} > H_{\mathrm{v},out} + d_{\mathrm{v},out}\ (fully\ submerged) \\ h_g - \left(\dfrac{H_{liq} - H_{\mathrm{v},out}}{d_{v,out}} \right) \left(h_g - h_f \right) & if\ H_{\mathrm{v},out} + d_{\mathrm{v},out} \geq H_{liq} \geq H_{\mathrm{v},out}\ (partially\ submerged) \\ h_g & if\ H_{liq} < H_{\mathrm{v},out}\ (unsubmerged) \end{cases}$$

(2.70)

3 Results and Validation

3.1 Alternative Refrigerant Evaluation Program

In recent years, an increased focus has been placed on replacing high Global Warming Potential (GWP) refrigerants with relatively low GWP alternatives. AHRI organized an industry-wide effort to evaluate the performance of candidate low-GWP refrigerants as drop-in replacements in existing systems for major product categories like air conditioners, heat pump, refrigerators etc.

One such study (Alabdulkarem et al., 2013) focused on residential heat pumps that use the refrigerant R410A, which has a GWP of 2,088 (IPCC, 2007). It evaluated the performance of three proposed alternatives: R32, D2Y60 (a mixture of 40% R32 and 60% R1234yf by mass) and L41A (73% R32, 12% R1234ze and 15% R1234yf by mass) for a variety of steady-state and cyclic tests against baseline performance for a 3-ton mini-split unit. The GWP values for these refrigerants is given in Table 3.1 below. The measured data from that study has been used as a basis for comparison of simulation results, focusing on two of the alternatives (R32 and D2Y60) along with the baseline refrigerant. The metrics used for comparison include suction and discharge pressure levels, compressor discharge temperature, indoor unit air-side capacities (and accumulated capacity for dynamic tests) and COP.

Table 3.1. Refrigerant GWP Values

Refrigerant	GWP Value
R410A	2088
R32	675
D2Y60	300
L41A	500

3.2 Experimental Facility

Figure 3.1 shows the schematic of the experimental facility set up for the performance evaluation of the heat pump. The outdoor unit was installed in an environmental chamber while the indoor unit was placed inside a wind tunnel. The environmental chamber was used to simulate ambient conditions and the indoor conditions were simulated inside the wind tunnel. A commercially-available R410A residential mini-split heat pump system was tested according to the ASHRAE test conditions outlined in standard 116-1995 (ASHRAE, 1995). Table 3.2 shows the test matrix for which simulations were compared against experimental results. The matrix includes both heating and cooling conditions in both steady-state and cyclic modes. The Extended test conditions are developed in-house. For the heating test, the extended conditions and the low temperature conditions could not be compared with simulations since not enough modeling data was available for these cases. Specifically, refrigerant mass flow rate measurements recorded were unrealistically low, and indoor unit outlet enthalpies could also not be calculated due to two-phase fluid present at the outlet. Thus capacity values could not be accurately determined.

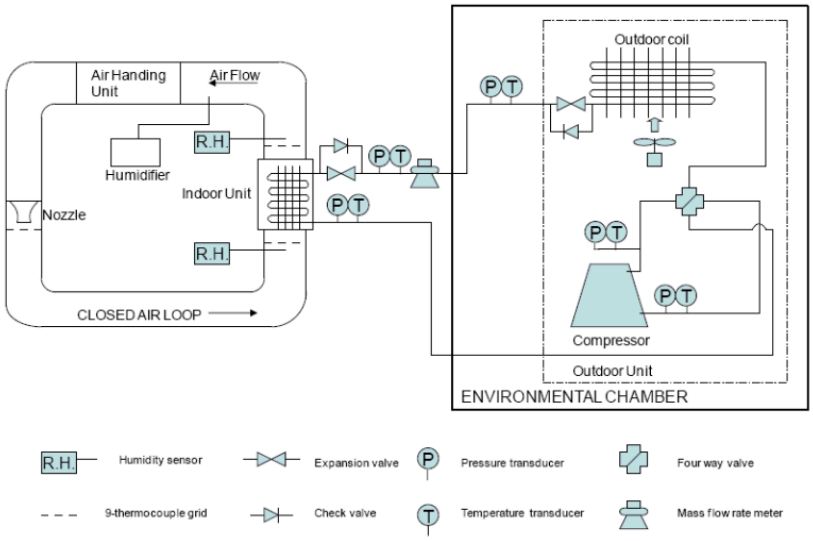

Figure 3.1. Experimental Facility Schematic

Table 3.2. ASHRAE Test Conditions

Test	Indoor		Outdoor		Operation
	DB	WB	DB	WB	
COOLING TESTS					
Extended	26.7°C	19.4°C	46.1°C	NA	Steady state
ASHRAE A			35.0°C		Steady state
ASHRAE B			27.8°C		Steady state
ASHRAE C		<=13.9°C	27.8°C		Steady state
ASHRAE D					Cyclic
HEATING TESTS					
High Temp 1	21.1°C	≤15.6°C	16.7°C	14.7°C	Steady state
High Temp 2			8.3°C	6.1°C	Steady state
High Temp Cyclic			8.3°C	6.1°C	Cyclic

Details of the instrumentation involved in the testing are listed in Table 3.3.

Table 3.3. Instrumentation Details

Instrument	Manufacturer	Range	Uncertainty
T-Type Thermocouple	Omega Engineering Inc.	-270°C to 400 °C	±0.5°C
Pressure Transducer	Setra Systems Inc.	0 to 3447 kPa	±0.11% full scale
Pressure Transducer	WIKA Inc.	0 to 6894 kPa	±0.125% full scale
Differential Pressure Transducer	Setra Systems Inc.	0 to 1.245 kPa	±1% full scale
Humidity Sensor	Vaisala	-40 to 80°C, 0 to 100%	±1%
Dew Point Sensor	General Easter	-80°C to 95°C	±0.2°C
AC Watt Transducer	Ohio Semitronics	0 to 5 kW	±0.5% full scale
AC Watt Transducer	Ohio Semitronics	0 to 300 V	±0.25% full scale
Mass Flow Meter	Micro Motion Inc.	0 tot 100 g/s	±0.15%

3.3 Component Details

The compressor used in this study is a fixed speed, R410A scroll compressor with a constant RPM of 3,500 and displacement of 27.62 cm^3/revolution. The outdoor unit is a fin-tube heat exchanger with a single bank of copper tubes using Aluminium extended surfaces. The indoor unit is a fin-tube A-coil heat exchanger with Aluminium fins and tubes, and has four banks of tubes. The heat exchangers are shown in Figure 3.2. The modeling parameters associated with the heat exchangers are given in Table 3.4

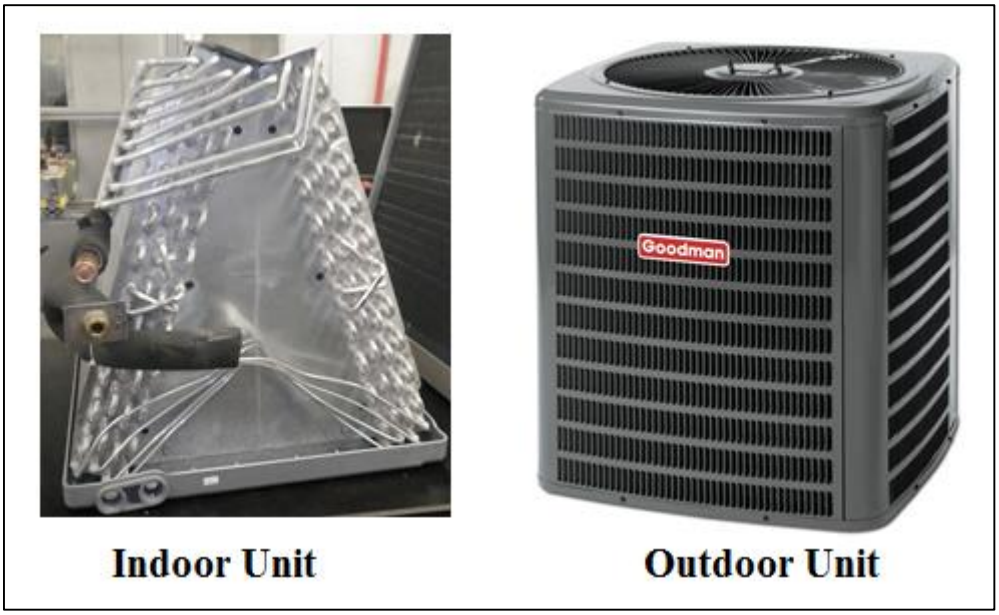

Figure 3.2. Heat Exchangers

For the heating modes, a simple fixed-diameter orifice is used as the expansion device, while for the cooling modes, a TXV is used. The discharge pipe is 2 meter in length, whereas the liquid and vapor line pipes are 10 meter in length. The modeling details are given in Table 3.5.

Table 3.4. Heat Exchanger Modeling Parameters

Parameter	Indoor Unit	Outdoor Unit	Units
Number of Tubes per Bank	22	36	
Number of Banks of Tubes	4	1	
Number of Parallel Coils	2	1	-
Tube Length	0.503	2.16	-
Tube Outer Diameter	9.5	9.5	-
Tube Thickness	8	8	m
Tube Vertical Spacing	0.02	0.025	mm
Tube Horizontal Spacing	0.025	0.025	mm
Tube Material	Aluminium	Copper	m
Fin Material	Aluminium	Aluminium	-
Fins Per Meter	590.55	826.77	1/m
Fin Thickness	0.1	0.1	mm

Table 3.5. Compressor and Valve Modeling Parameters

Parameter	Value	Units
Compressor		
Displacement	27.62	cm^3/rev
RPM	3,500	rev/min
Thermostatic Expansion Valve		
Orifice Diameter	3.86	mm
Rod (Stem) Diameter	2.69	mm
Pin Diameter	4.74	mm
Pin Height	1.25	mm
Minimum Opening Area	1.00E-06	m^2
Flow Coefficient	0.28	-
Valve Time Constant	90	s
Initial Spring Force	1.50E+05	N/m^2
G-Factor	1.50E+08	N/m^3
Fixed Diameter Orifice		
Orifice Diameter	2.0	mm
Flow Coefficient	0.28	-

3.4 Model Implementation

The system model as implemented on the Simulink® platform is shown in Figure 3.3 for the heating mode. The components are drag-and-drop in nature, and are connected to each other in the order shown. For the connections between the components, the two-way connection blocks available in the SimScape™ toolbox are employed. These connectors allow signals to propagate information in both directions. A combination of two solvers was used for running the simulation. ode45 (Dormand and Prince, 1980), with a relative tolerance of 1e-6, and the maximum time step limited to 0.001 seconds, and the stiff solver ode23tb with a relative tolerance of 1e-8 and a maximum time step of 0.001 seconds (Hosea and Shampine, 1996).

While the actual system uses a combination of check valves and reversing valves to switch between heating and cooling modes, separate simulations models were created for the heating and cooling cases to maintain simplicity. The cooling mode utilizes a TXV to control suction superheat, whereas the heating mode uses a fixed-diameter orifice.

Heat transfer coefficients for the refrigerant-side are calculated for steady-state conditions and provided as inputs to the model. For the air-side, the correlation developed by Wang et al. (2000) for plain fin and tube heat exchangers is used for both the indoor and outdoor units.

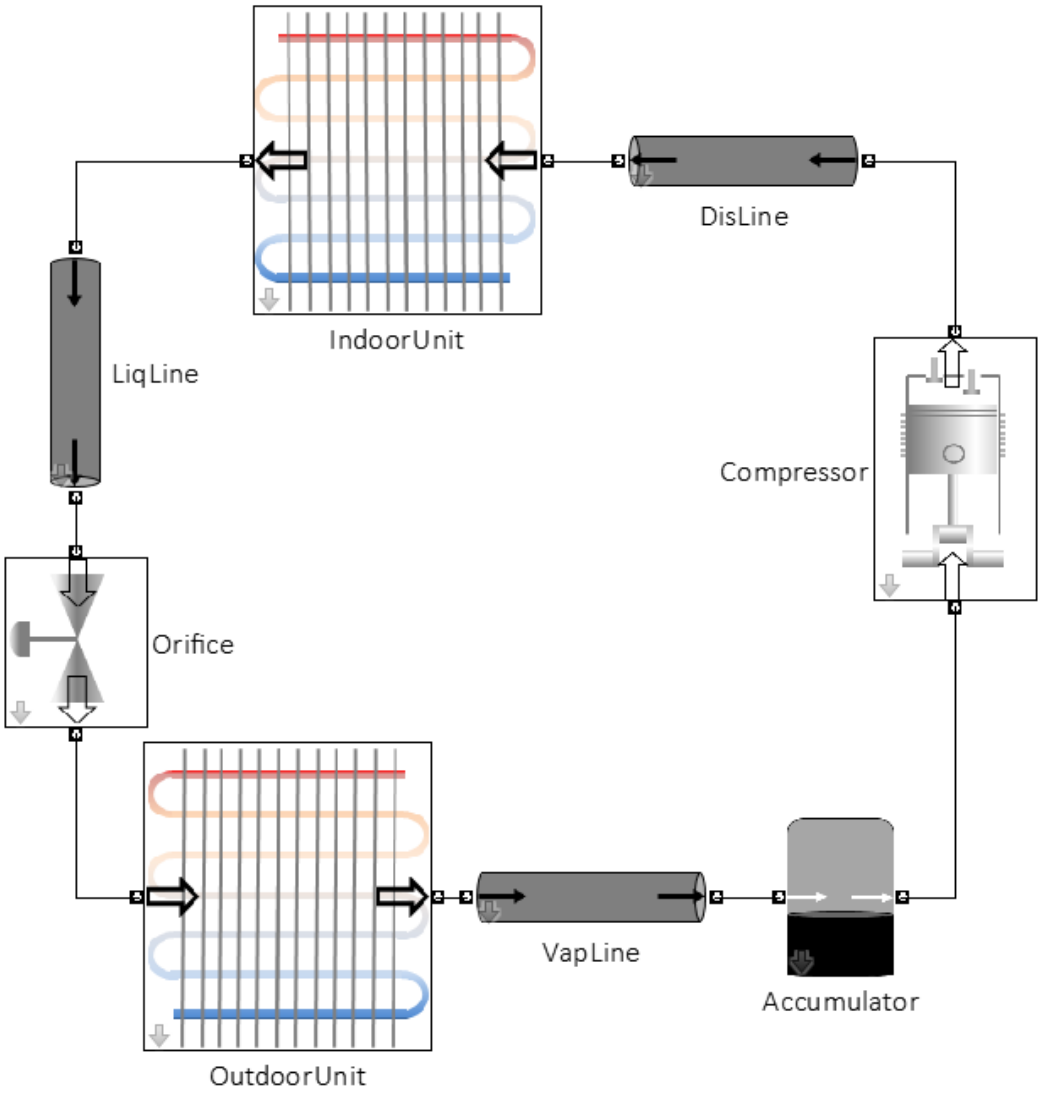

Figure 3.3. Simulink® Model (Heating Mode)

Under startup and shutdown conditions, the compressor RPM is assumed to vary linearly, with an assumption of 10 seconds to cycle between operating states. This value is arbitrarily chosen due to the difficulty in obtaining accurate compressor speed measurements. The isentropic and volumetric efficiencies are calculated using experimental data and fed as inputs to the model. For the cyclic tests, the ambient

conditions match steady state tests (for the cooling tests, the ASHRAE C test and the D test share ambient conditions whereas for the heating tests, the High Temperature 2 test and the High Temperature Cyclic tests share ambient conditions). The values from the corresponding steady-state tests are used as inputs for the cyclic tests.

For the thermostatic expansion valve model, the geometry parameters from an available model of similar capacity are used as inputs due to the difficulty in obtaining data of the actual valve.

The indoor unit is modeled as two parallel coils, with the air and refrigerant side mass flow being evenly split between the two coils. The initial conditions used for the cyclic simulations are taken using the conditions of the experimental system after the 24 minute shutdown period. For steady-state simulations, an approximate equilibrium pressure is assumed, and initial vapor qualities are approximated to get the correct total refrigerant charge.

An important consideration while simulating physical systems is error propagation. An error in an input parameter might be amplified and lead to larger errors in predictions of system performance. However, for a dynamic simulation tool, the steady-state results represents bounds on the system, and the importance of such errors is reduced. Nevertheless, to analyze the sensitivity of parameters, a sample testing of the heat exchanger component was performed, using a correction factor for the air-side heat transfer coefficient. The coefficient was varied by ±20% and ±10% and the impact on capacity was compared. The result is shown in Figure 3.4 below.

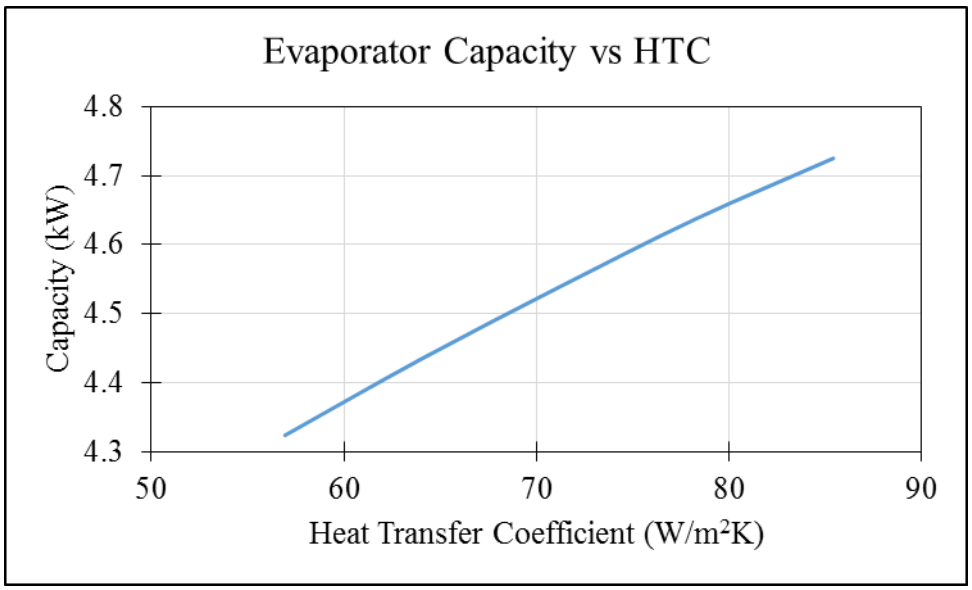

Figure 3.4. Air-Side Capacity vs Heat Transfer Coefficient

It can be seen that the trend is nearly linear. Thus, a change in heat transfer coefficient on the air side can significantly affect the capacity value. This trend may be expected since the air side limits the heat transfer rate of the heat exchanger. This also justifies the decision to use correlations for calculating air-side HTC, although refrigerant side are provided as inputs for a nominal mass flow rate.

3.5 Charge Optimization

In the experimental work, charge optimization studies were performed to evaluate an optimal charge values. Optimal charge value was defined as the conditions in which maximum COP was obtained. ASHRAE A-test conditions were used for the studies. Corresponding simulation studies were carried out to evaluate optimal simulation charge values and the results were compared with measured data. Discrete values of charge were used spaced approximately 400 g apart, to reflect experimental testing, although it is easily possible to conduct such a study with a much finer mesh.

Additionally, it is important to note that, due to the inability to account for the entire volume of the experimental unit, as well as a homogeneous flow model assumption for two-phase fluid, the predicted charge in the simulation will be less than actual system charge. This is often found to be the case in dynamic simulations of such systems (Bendapudi, 2008 and Qiao, 2014 for example).

For the baseline refrigerant, charge was varied between 2.23 kg and 3.80 kg. The optimum charge was found to be 3.02 kg. Similarly, for R32, the charge was varied from 1.60 kg to 3.20 kg with optimal performance at 2.00 kg, and for D2Y60, the variation was from 2.02 kg to 3.60 kg. Optimum value of charge was found to be 2.80 kg. Figure 3.7, Figure 3.6 and Figure 3.7, show the results. In the subsequent steady-state and transient tests, the refrigerant mass has been limited to within 0.1% of the actual optimized value since it is difficult to ensure that charge inventory matches the optimum value exactly. The optimization results are listed in Table 3.6.

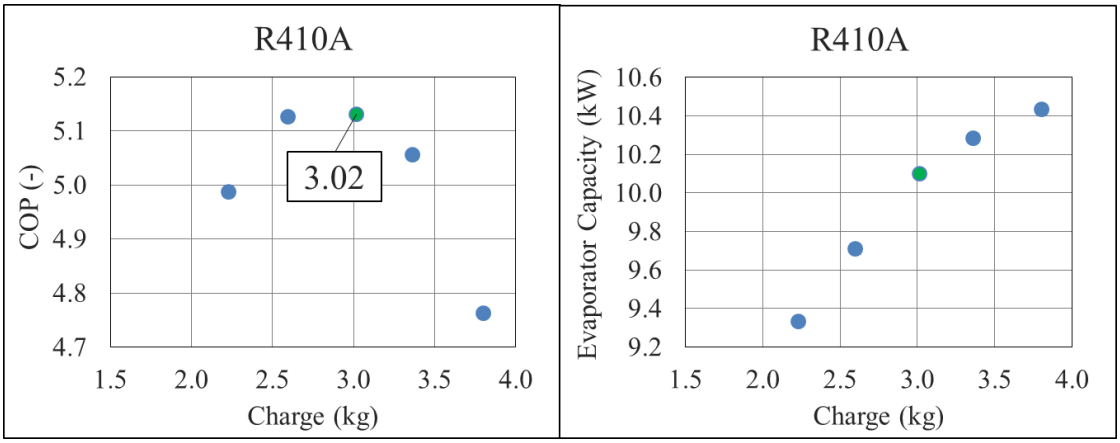

Figure 3.5. R410A Charge Optimization

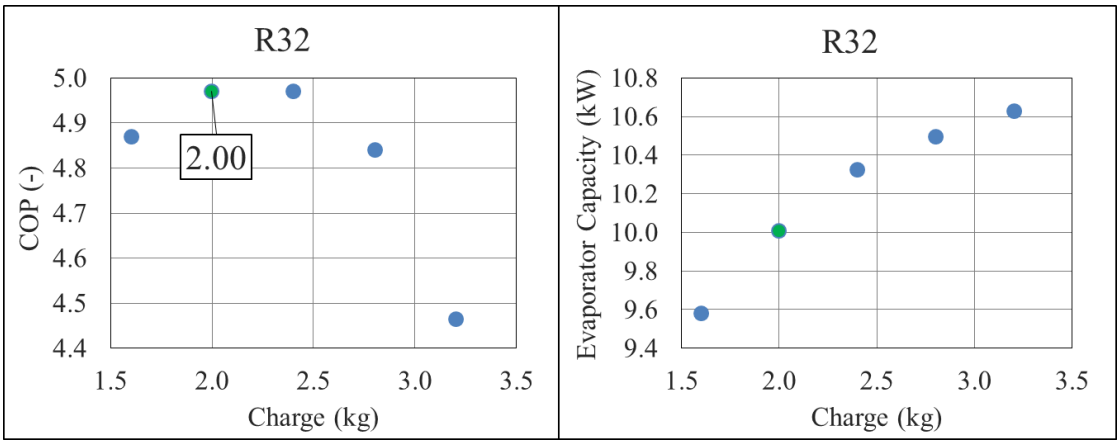

Figure 3.6. R32 Charge Optimization

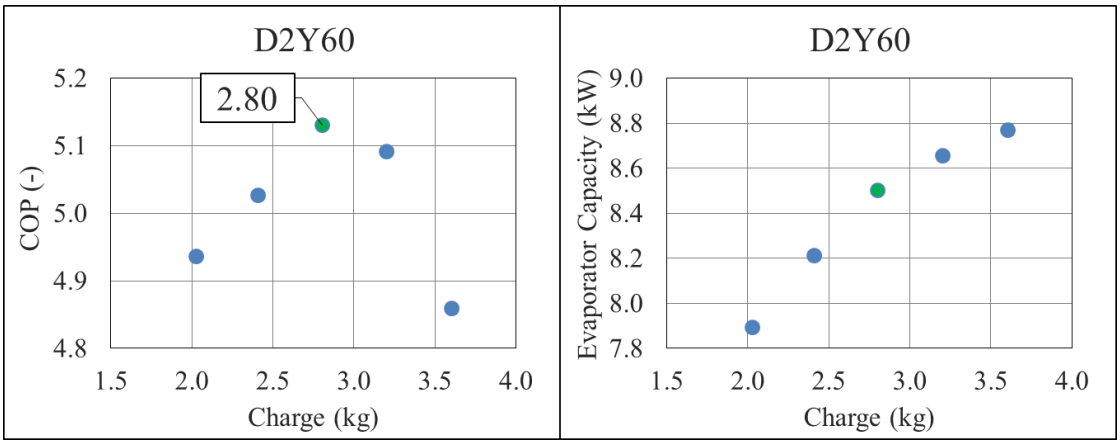

Figure 3.7. D2Y60 Charge Optimization

Table 3.6. Charge Optimization Results

R410A			
Charge (kg)	Capacity (kW)	COP (-)	Dis. Temp (°C)
2.23	9.33	4.99	81.0
2.59	9.71	5.13	81.6
3.02	10.10	5.13	84.6
3.36	10.29	5.06	87.2
3.80	10.44	4.76	93.2
R32			
Charge (kg)	Capacity (kW)	COP (-)	Dis. Temp (°C)
1.60	9.58	4.87	93.6
2.00	10.01	4.97	96.5
2.40	10.33	4.97	100
2.80	10.50	4.84	104.3
3.20	10.63	4.46	113.9
D2Y60			
Charge (kg)	Capacity (kW)	COP (-)	Dis. Temp (°C)
2.02	7.90	4.94	73.4
2.41	8.21	5.03	73.9
2.80	8.50	5.13	74.7
3.20	8.66	5.09	76.4
3.60	8.77	4.86	80.5

3.6 Steady-State Results

To simulate steady-state test conditions, approximate equilibrium initial conditions attained after shutdown have been used. The system is then allowed to run until time-invariant conditions are established, and the final state values are used for comparison purposes. Steady-state conditions serve as a 'proving grounds' for the models prepared, and acceptable steady-state results show a readiness for the complete cyclic simulations.

The system COP has been calculated using the following correlation:

$$COP = \frac{\dot{m}_{ref}\left(h_{indoor\,unit,out} - h_{indoor\,unit,in}\right)}{\dot{m}_{ref}\left(h_{compressor,out} - h_{compressor,in}\right)} \qquad (2.71)$$

The comparison for COP for combined heating and cooling results are shown in Figure 3.8. It is seen that the COP values match well with experimental data, with the deviation being within ± 8% for all conditions. The relative COP trends between the refrigerants are correctly predicted for all steady state conditions, except for the extended condition. For the extended test, while the experiments reveal that R32 has slightly higher COP than baseline, and D2Y60 is highest, the simulations reveal that R32 will have slightly lower COP. However, the absolute value of the COP itself is very small and therefore the margin for error is smaller for the test.

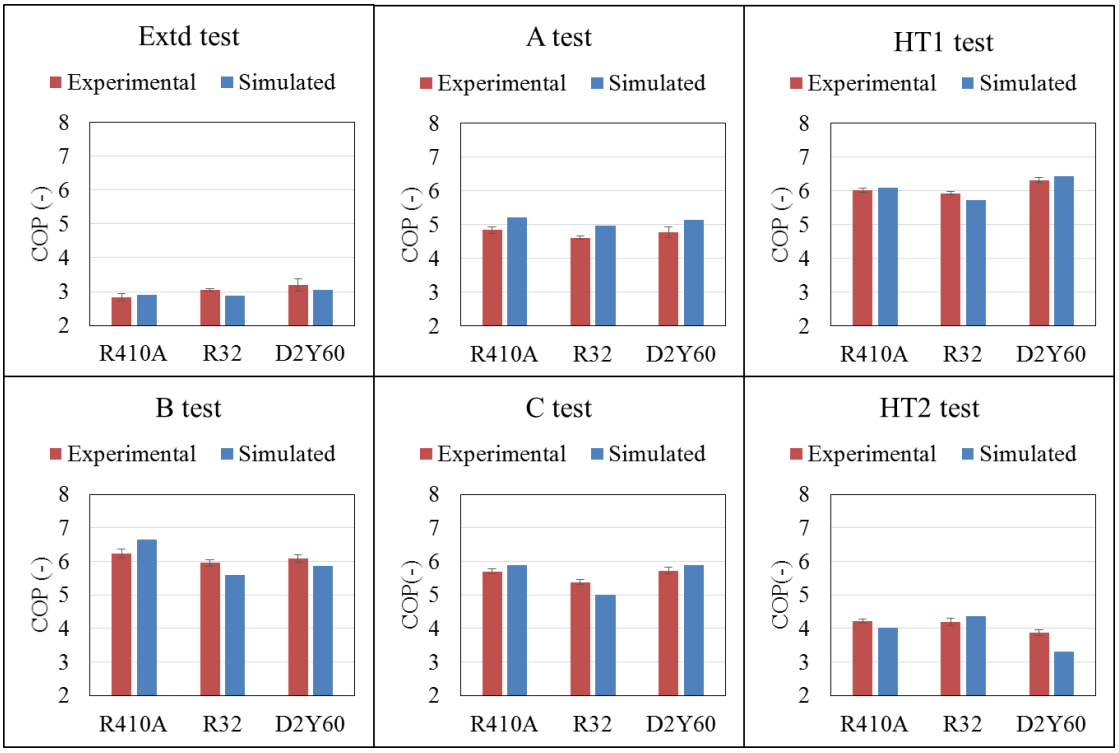

Figure 3.8. COP Comparison for Steady-State Tests

3.7 Transient Test Results

The ASHRAE cyclic tests are performed by running the compressor for 6 minutes followed by 24 minutes of compressor-off time. Typically, the on/off cycles

are successively repeated several times, and the last complete cycle is used. The cooling results are discussed first followed by the heating results.

3.7.1 Cooling Test Results

The results for the ASHRAE D-test are discussed in this section. The suction and discharge pressures for the three refrigerants are shown in Figure 3.9. It can be seen that R32 operates at similar pressure levels as R410A, while D2Y60 has lower suction and discharge pressures than the other two refrigerants. R410A shows a large divergence on the discharge pressure side. This occurs due to the accumulator initially containing some liquid which eventually evaporates. Initially, while there is still liquid inside the accumulator, the outlet vapor is saturated. Once the accumulator empties out, the outlet vapor starts to be superheated, leading to a higher discharge pressure and temperature. The combination of inadequate initial charge distribution values for the system, along with the lack of TXV modeling data implies that the valve operation is difficult to predict.

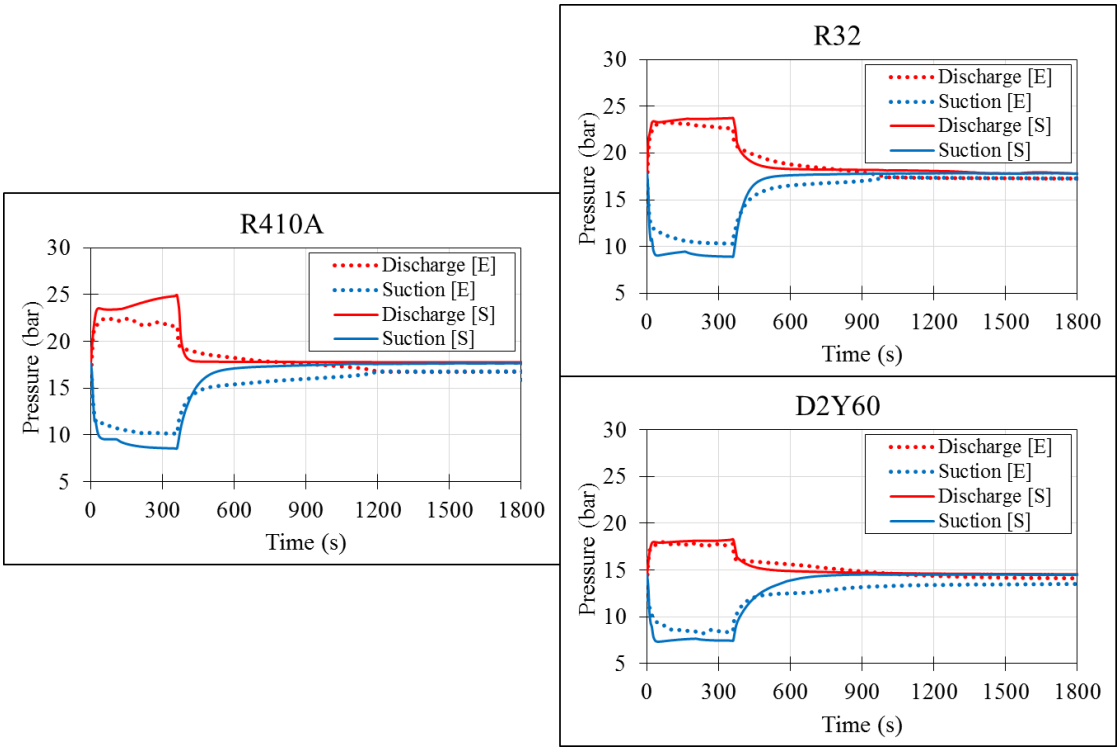

Figure 3.9. Comparison of Suction and Discharge Pressures Under D-Test Conditions

The three discharge temperatures are shown in Figure 3.10. R32 has the highest discharge temperature, about 10K higher than D2Y60 at the peak values. For the R32 and R410A cases, the simulations significantly overpredict the discharge temperature. In addition, the cooling trend of discharge temperature upon shutdown is also faster than experiment. The difficulty in evaluating the thermal mass of the compressor leads to the difficulty in accurately modeling the heat transfer inside the compressor shell, and thus, it is difficult to predict the discharge temperatures with high accuracy. Additional details about the internal geometry of the compressor would results in a more accurate heat transfer model to the compressor shell.

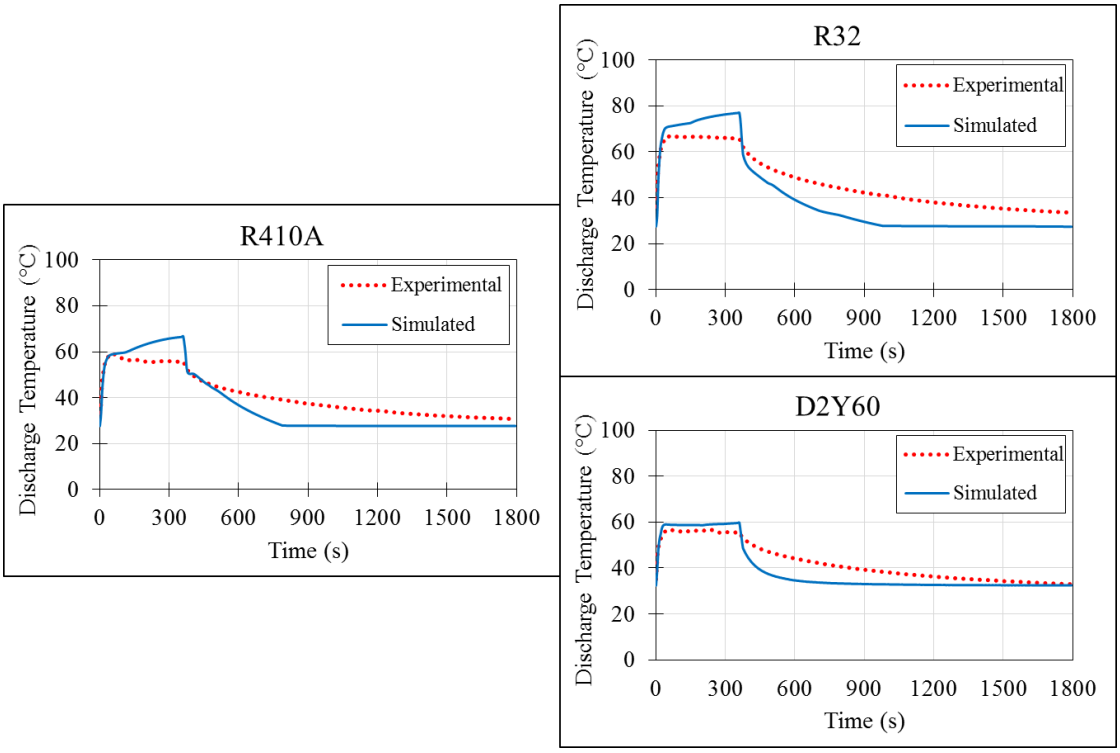

Figure 3.10. Comparison of Discharge Temperatures Under D-Test Conditions

The air side cooling capacities for the indoor unit are shown in Figure 3.11. The simulated accumulated capacities for R410A, R32 and D2Y60 are 0.802, 0.814 and 0.674 kW-hr, respectively. The differences are shown in Table 3.7. The simulation predictions match experimental data in terms of the relative comparisons between the refrigerants, with R32 showing slightly higher capacity than R410A, and D2Y60 being significantly lower than the other two.

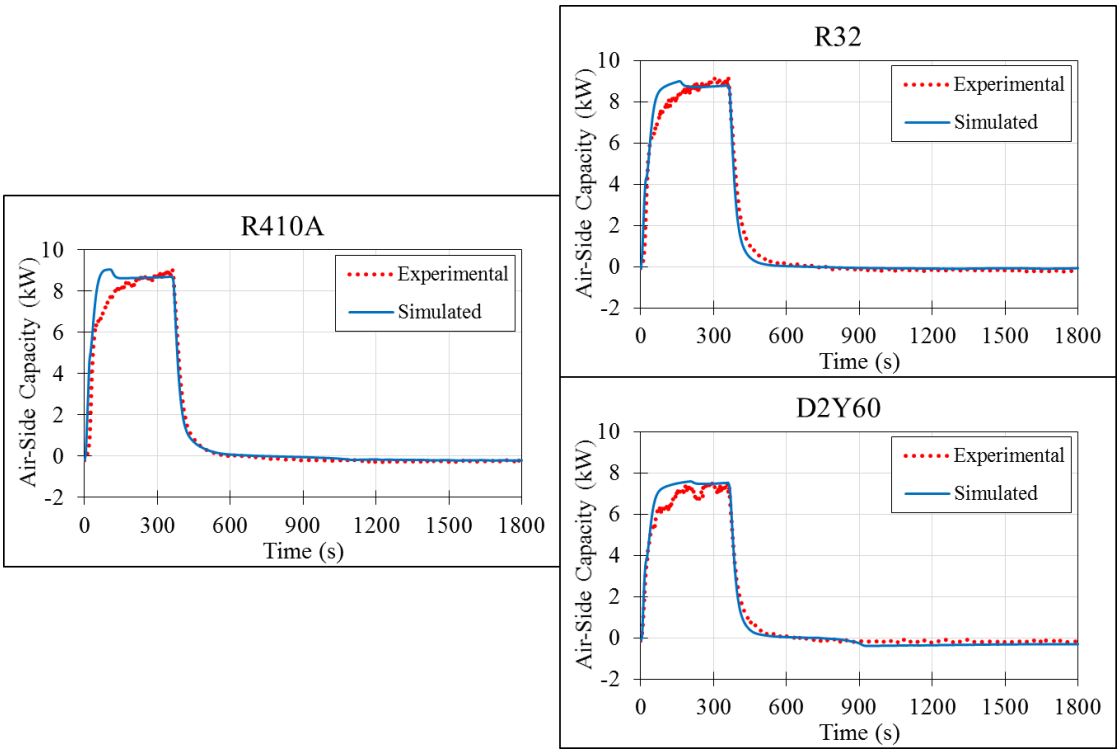

Figure 3.11. Comparison of Indoor Unit Air-Side Capacities Under D-test Conditions

Table 3.7. Comparison of Accumulated Capacities Under for D-test

Refrigerant Name	Accumulated Capacity (kW-hr)	Error (%)
R410A	0.802	7.66
R32	0.814	5.94
D2Y60	0.674	5.62

In addition to capacity comparisons, the power consumption of the unit is also of interest. During the experimental study, the fan on the indoor unit was removed, and instead, the wind tunnel blower was used to force air across the heat exchanger. The fan power for the indoor unit was accounted for using power consumption data for the fan available from the manufacturer, with an average value of 373 W being considered for all cases. The current simulations model do not account for fan power, therefore, this value has been added to compressor power to get the total power consumption. The

results are shown in Figure 3.12. It is seen that compressor power is well predicted for the alternatives, although the divergence that was observed for discharge temperature manifests itself as an increase in compressor power for R410A also. The accumulated power consumption is shown in Table 3.8.

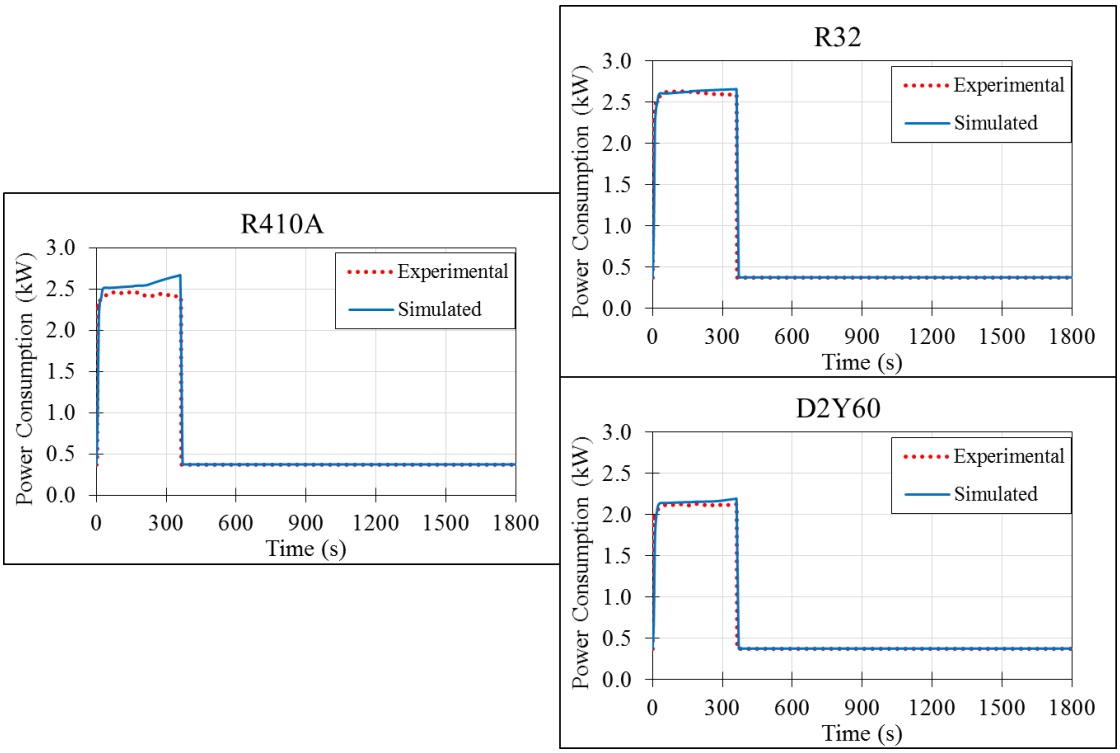

Figure 3.12. Comparison of Power Consumption Under D-test Conditions

Table 3.8. Comparison of Accumulated Power Consumption for D-test

Refrigerant Name	Accumulated Power Consumption (kW-hr)	Error (%)
R410A	0.253	4.9
R32	0.260	0.2
D2Y60	0.211	-1.0

The refrigerant mass distribution is shown in Figure 3.13. While all components have a small control volume, and thus store a certain amount of charge, they are often small for certain components and not relevant in discussions. These components,

specifically the orifice/TXV, discharge line and the vapor line, have not been shown for the sake of simplicity. As expected, most of the refrigerant mass during on-time is inside the outdoor unit, since it is operating at a higher pressure, with almost 50% of refrigerant making its way to the outdoor unit. After shutdown, refrigerant tends to collect in the coldest parts of the cycle, which is the indoor unit in this case. This trend can also be seen in the plots below. Some charge also migrates to the accumulator after shutdown. It is worth noting that the simulations do not account for gravitational effects. In the experiment, the indoor unit was mounted much higher than the accumulator, and some charge would likely flow out of it into the accumulator, but this trend cannot be accounted for.

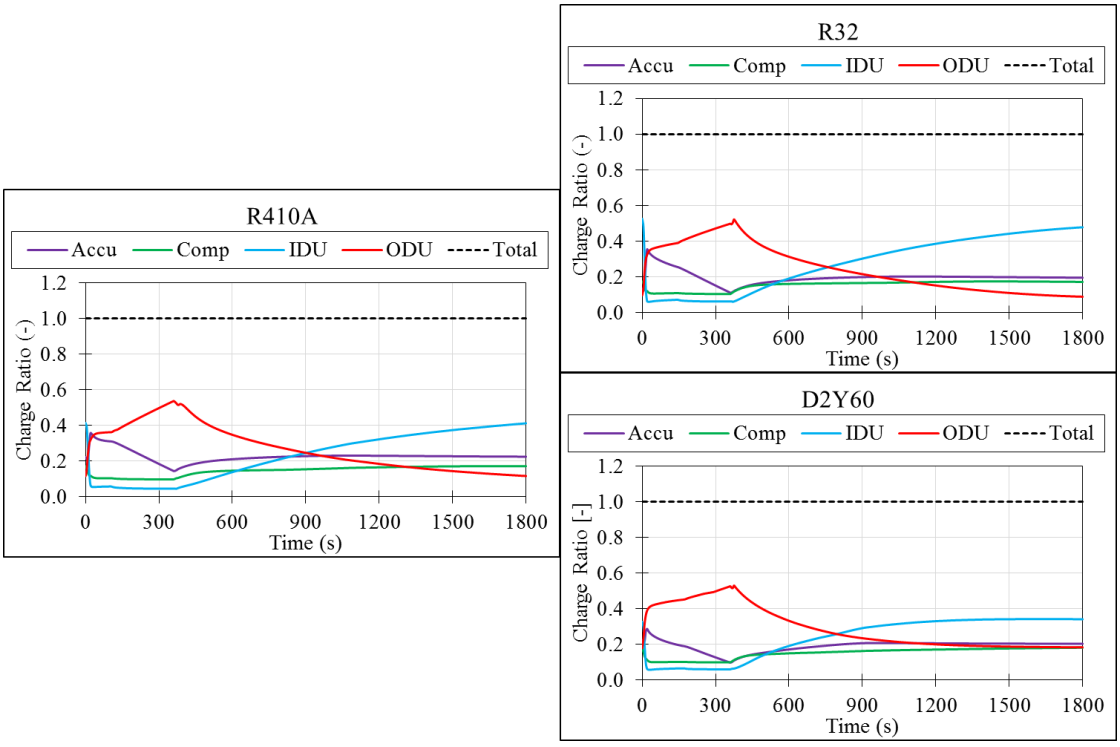

Figure 3.13. D-Test Refrigerant Mass Migration

3.7.2 Heating Test Results

The suction and discharge pressures for R410A, R32 and D2Y60 are shown in Figure 3.14. It can be seen that the simulations predict the pressure levels and transient trends. While R410A and R32 have similar pressure levels, D2Y60 has lower discharge pressure than both. After shutdown, the simulations show a faster equalization of pressure levels compared to measurements. This is likely due to the approximate tuning of the fixed orifice instead of having physical data available.

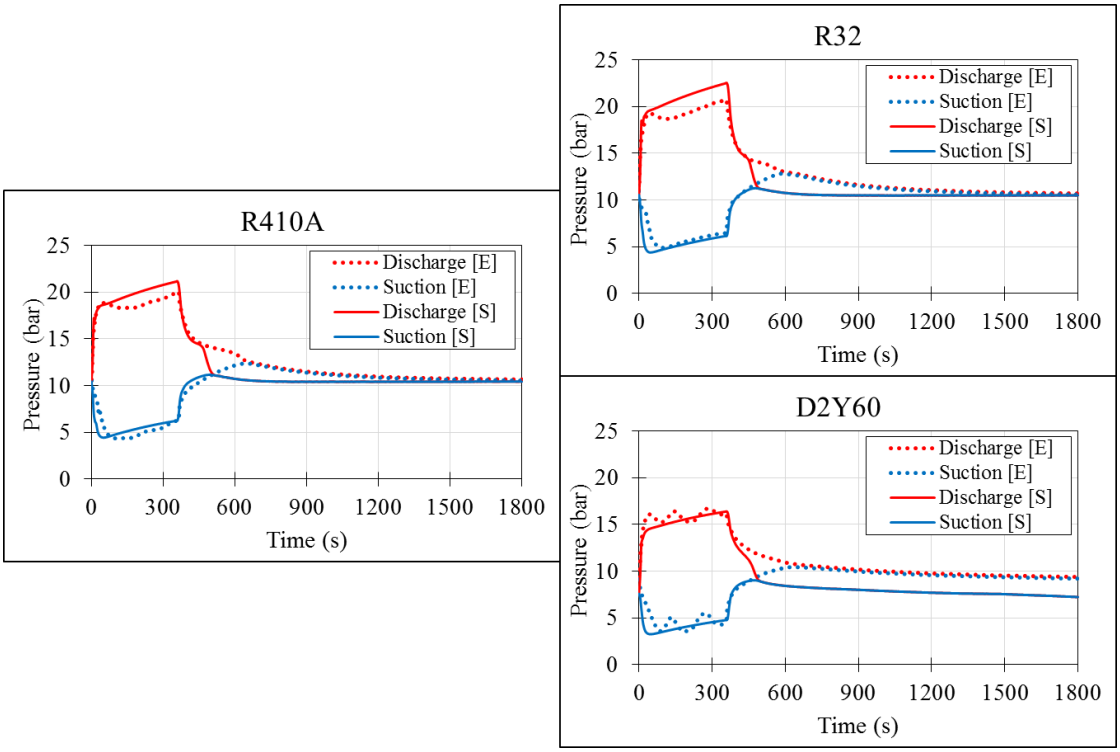

Figure 3.14. Comparison of Suction and Discharge Pressures Under Heating Cyclic Test

Figure 3.15 shows the comparison of compressor discharge temperature. It can be seen that the simulations predicts the peak discharge temperature with reasonable accuracy. However, the on-cycle transient behavior is slightly different, with the simulated temperature gradually increasing to a maximum just before shutdown,

whereas during the experiments, the temperatures peaked relatively quickly and then decreased slightly until shutdown. This deviation is due to the inability of accurately modeling the heat transfer to the compressor shell, due to lack of information about the compressor geometry. The results also show that R32 has considerably higher discharge temperature than R410A, while D2Y60 is similar to R410A. These trends were also witnessed in the cooling cyclic test.

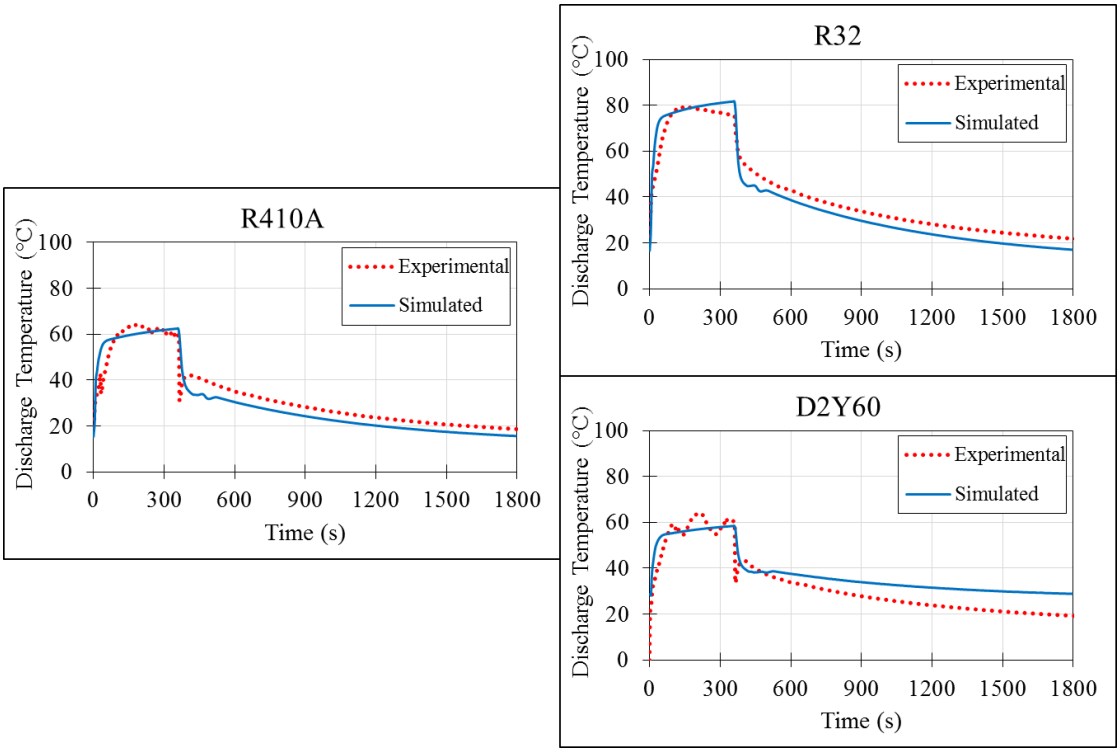

Figure 3.15 Comparison of Discharge Temperature Under Heating Cyclic Test

Figure 3.16 shows the comparison for air side capacities of the three refrigerants. The simulated accumulated capacities for R410A, R32 and D2Y60 are 0.545, 0.495 and 0.441 kW-hr, respectively. The accumulated capacity differences between experimental data and simulations for R410A, R32 and D2Y60 are 8.7%,

1.4% and 7.8%, respectively. The measured data shows unexplained fluctuations observed for the D2Y60 test.

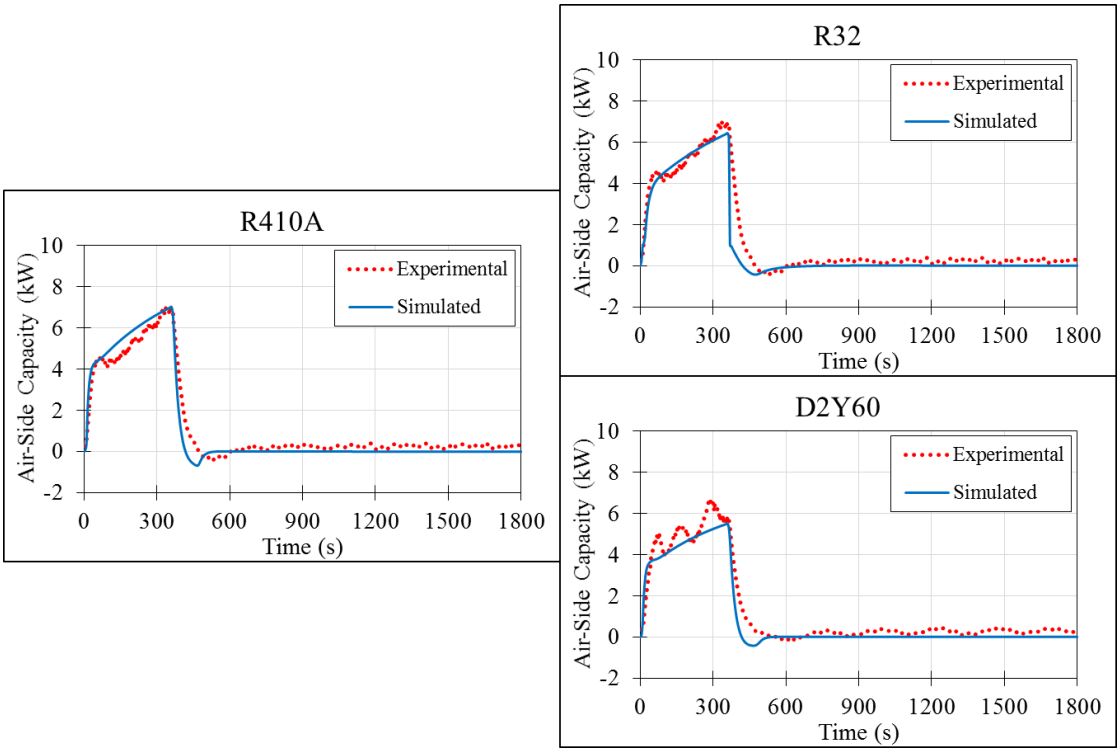

Figure 3.16. Comparison of Indoor Unit Air-Side Capacities Under Heating Cyclic Test

Table 3.9. Comparison of Accumulated Capacity for Heating Cyclic Test

Refrigerant Name	Accumulated Capacity (kW-hr)	Error (%)
R410A	0.545	8.68
R32	0.495	-1.38
D2Y60	0.441	-7.85

The comparison for power consumption is shown in Figure 3.17. The trends appear to differ from the experiment, with the simulations showing a gradual of power consumption, although the measurements show a roughly-constant-to-slightly-increasing trend. The differences of accumulated power consumption are listed in

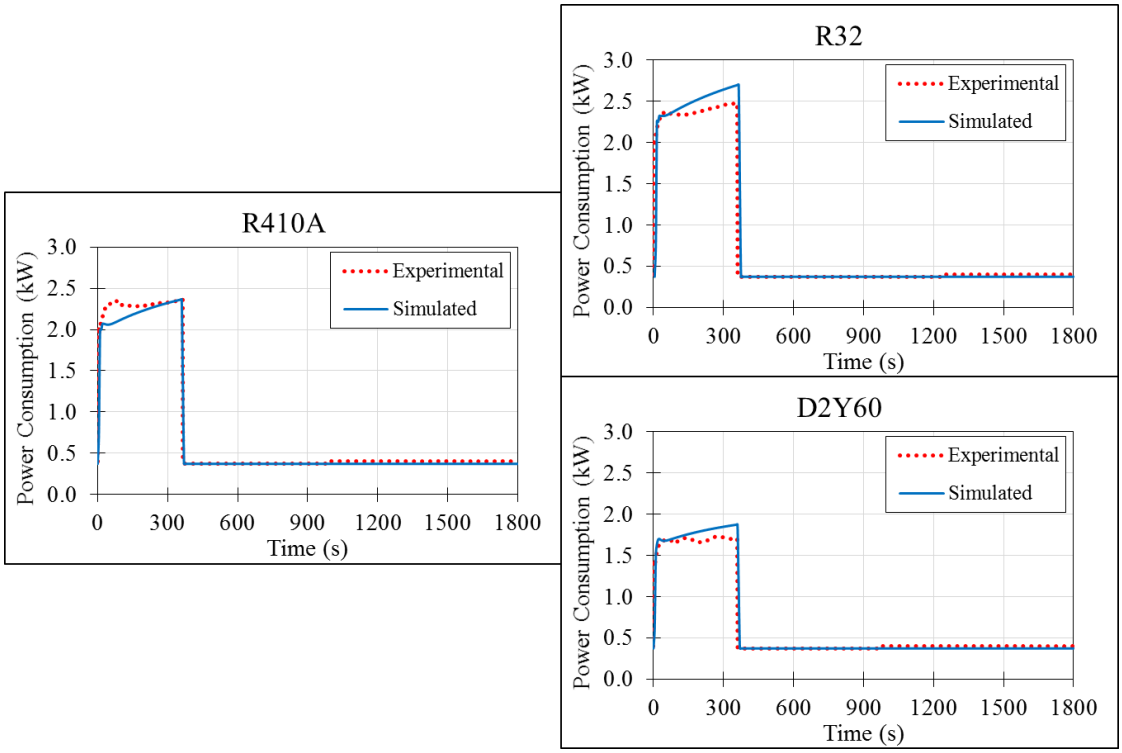

Figure 3.17. Comparison of Power Consumption Under Heating Cyclic Test

Table 3.10. Comparison of Accumulated Power Consumption for Heating Cyclic Test

Refrigerant Name	Accumulated Power Consumption (kW-hr)	Error (%)
R410A	0.219	-4.5
R32	0.208	0.2
D2Y60	0.176	4.4

Figure 3.18 shows the refrigerant mass migration for the three refrigerants. It can be seen that, during the six minutes compressor-on state, the refrigerant is still migrating and does not reach a steady state condition. Upon shutdown, the refrigerant collects in the cooler part of the cycle, with the majority settling in the accumulator. The indoor unit has hotter ambient conditions compared to the outdoor components, and thus, charge migrates out of the indoor unit. This is different to the cooling tests

where the coldest ambient conditions exist at the indoor unit and thus refrigerant migrates to the indoor unit upon shutdown. It can also be seen that the total charge is conserved.

The results cannot be compared to measured data due to the difficulty of measuring charge inventory within individual components. However, the plots are able to give insight into the behavior of the refrigerant under dynamic conditions.

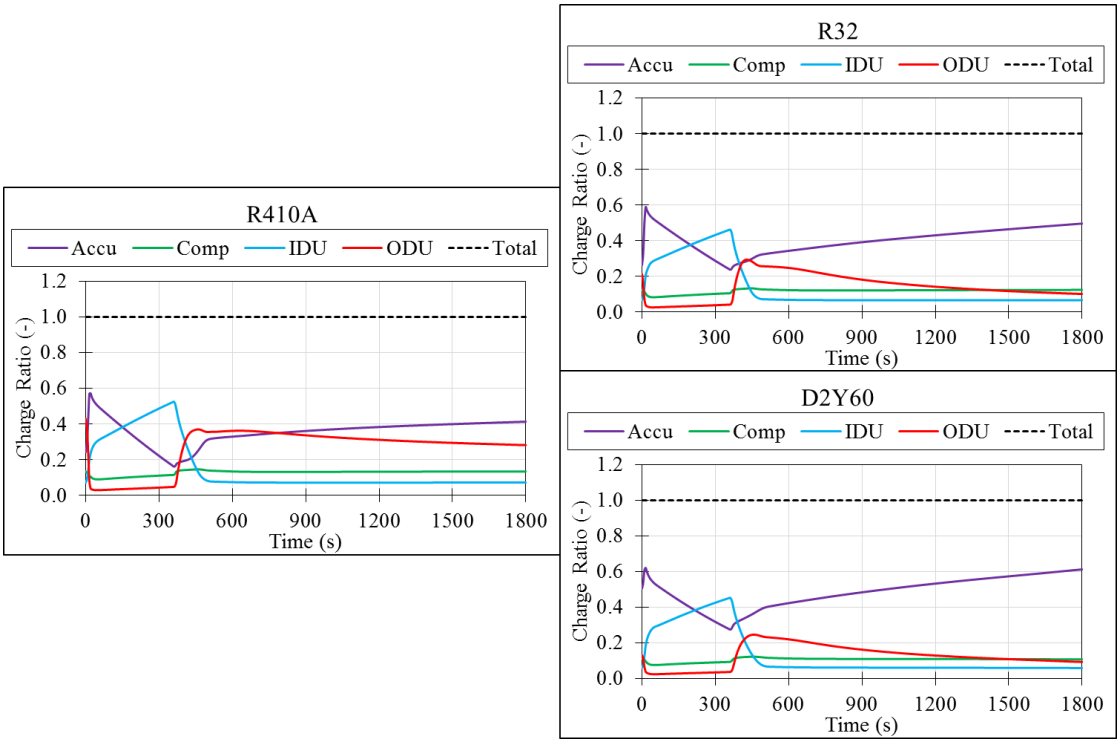

Figure 3.18. Heating Cyclic Test Refrigerant Mass Migration

3.8 Discussion

The results show that R32 has higher cooling capacities in several steady-state tests, and also larger accumulated capacity in the cyclic test. However, R32 also shows lower COPs for the tests. This is due to the lower compressor efficiencies for R32. Also, R32 shows a consistently higher discharge temperature than the baseline refrigerant.

D2Y60 shows lower capacities than R410A in all cases, although has comparable COPs to the baseline.

For the heating tests, R32 shows higher capacities for both the steady-state test conditions tested. However, as in the cooling case, the COP of R32 is lower. D2Y60 shows lower capacities than baseline, and lower COP for the HT1 test, although COP is comparable for the HT2 test. These findings are consistent with the findings of the experimental testing.

From the above results, it is seen that it is possible to optimize the refrigerant mass individually for each alternative refrigerant to obtain an optimal COP. A range of parameters can be compared such as suction and discharge pressures, discharge temperatures, indoor unit capacity and power consumption of the unit. These parameters all play a role in the evaluation of an alternative when being used in a real-life system.

A significant factor to keep in mind is that while the alternatives offer lower GWP values, these values only affect direct emissions of a system. Depending on the capacity and COPs obtained, the overall power consumption of the unit might be higher or lower, and a full scale LCCP analysis might be necessary to evaluate whether a proposed candidate represents real savings in greenhouse gas emissions.

4 Conclusions

This thesis describes the development of a component-based framework in Simulink® for the dynamic simulation of vapor compression heat pumps. The framework includes the most commonly used components in such systems. The components are designed to have the same boundary conditions, allowing them to be inter-connected in arbitrary fashion.

The framework has been used to simulate the performance of a residential heat pump under both steady-state and dynamic operating conditions, in both heating and cooling modes. The baseline refrigerant performance has been compared to the performance of potential drop-in replacement candidates R32 and D2Y60. In addition, charge optimization studies have been carried out to show that optimal charge values that give highest COP exist for the investigated refrigerants. The results of the simulations show that R32 typically has lower COPs compared to the baseline case, which may be expected since the compressor has been designed for R410A operation. R32 shows slightly higher capacities than R410A in some cases. In addition, R32 consistently shows higher discharge temperatures, which may negatively affect the life of compressor components. While D2Y60 often has comparable COPs to the baseline, it usually shows reduced system capacities, which affects the heating or cooling loads that the system can handle.

The simulations compare well against measured data, with the errors in accumulated capacity being generally under 10%. The pressure levels and the startup/shutdown trends are also reproduced well. Significantly, the relative comparisons in terms of the performance *between* the different refrigerants is also

reproduced, indicating that the models can predict performance differences between alternative fluids. The comparison to the experimental data shows that the framework is capable of simulating reasonably complicated cycles featuring valves, multiple pipes and an accumulator and reproduce steady-state data and transient trends with acceptable accuracy. However, the lack of availability of TXV data and compressor internal construction details mean that some trends, such as discharge temperature, cannot be reproduced closely.

4.1 Contributions

In developing the framework, this thesis has lead to the following major contributions:

- A component-based library has been developed in Simulink® that allows the simulations of vapor compression cycles with arbitrary cycle configuration
- The framework contains the most commonly-used components in vapor compression systems including a fin-tube heat exchanger, map-based and efficiency-based compressors, TXV, EEV and reversing valves, accumulator/receiver, flash tank and pipe models
- The framework can be used for simulating start-up and shutdown transient phenomena. External models for thermal zones can also be connected to the heat exchanger to simulate transient changes to the supply air. In addition, user-defined models can be used to control compressor/fan operation
- The framework has been used to evaluate the performance of alternative low GWP refrigerants when used as drop-in substitutes for an R410A for a residential heat pump. The models are capable of giving useful insights in terms of comparisons between discharge temperatures, pressures and capacities.

Complete startup and shutdown cycles have been simulated, and the framework shows no problems in dealing with zero mass flow rates. Refrigerant mass migration trends can also be evaluated, which are relevant when understanding cycling losses.

- The low GWP comparison tests have also been used to validate the library. It is found that the models can predict steady state performance parameters within 10% error. For the cyclic tests, the accumulated capacity errors are found to be within 10% of measured data for 7 of the 8 transient tests simulated
- Only known work in open literature evaluating performance of low-GWP refrigerants under dynamic conditions
- Journal: Ling, J., Bhanot, V., Alabdulkarem, A., Aute, V., Radermacher, R., *"Transient Simulation of Heat Pumps Using Low GWP Refrigerants",* Science and Technology for the Built Environment, 2015, DOI:10.1080/ 23744731.2015.1034044
- Conference: Bhanot, V., Bacellar, D., Ling, J., Alabdulkarem, A., Aute, V., Radermacher, R., "*Steady-State and Transient Simulations of a Vapor Compression Cycle Using Simulink",* International Conference on Refrigerators and Air Conditioners, Purdue, 2014

4.2 Future Work

While the current framework provides a good foundation for the modeling and simulation of vapor compression systems under transient conditions, additional work in the field can further enhance the usefulness of the framework

- A validated moving boundary heat exchanger model with switching schemes. Moving boundary models are lower-order compared to finite volume models, sacrificing model flexibility in favor of model simplicity. This trait is desirable in control-oriented modeling where the focus is on the dynamic trends and fast simulations rather than high accuracy. In addition, for the finite volume model, frosting and defrosting phenomenon should also be modeled.
- Investigation into the capabilities of Matlab/Simulink solvers. Vapor compression systems are stiff systems by nature and require robust ODE/DAE solvers for their simulations. During the course of this work, numerical issues were often faced in attempting to integrate the relevant DAEs in Simulink in semi-explicit forms. Further research into this topic may reveal useful methods for improving solver performance.
- Further validation work of more complicated cycles. Specifically, a flash tank vapor-injection (FTVI) cycle has been experimentally investigated and transient test data is available. The dataset should be used to validate the more complicated FTVI cycle. In addition, datasets for Variable Refrigerant Flow (VEF) systems are also available and should be used for further validations.
- Accounting for flow splitting and merging phenomena. Currently, parallel components cannot be simulated. However, to simulate complete heat pump units, check valves connected in parallel to expansion devices will need to be modeled to account for reversing of flow between heating and cooling cases, and also when simulating defrost cycles.

5 References

[1] ANS/AHRI Standard 540. *Performance rating of positive displacement refrigerant compressors and compressor units.* Arlington, VA: Air-conditioning, Heating and Refrigeraiton Institute, 2004.

[2] ANSI/ARI Standard 116-1995: *Methods of Testing for Rating Seasonal Efficiency of Unitary Air Conditioners and Heat Pumps*. Atlanta: American Society of Heating, Refrigerating and Air-Conditioning Engineers Inc., ASHRAE, 1995.

[3] Alabdulkarem A., Hwang Y., Radermacher R., System Drop-In Tests of Refrigerants R-32, D2Y-60, and L-41a in Air Source Heat Pump, *Air-Conditioning, Heating, and Refrigeration Institute*, Low-GWP Alternative Refrigerants Evaluation Program, 2013.

[4] Aute, V., Radermacher, R., *Standardized Polynomials for Fast Evaluation of Refrigerant Thermophysical Properties,* International Refrigeration and Air Conditioning Conference at Purdue, 2014.

[5] Bendapudi, S.A., and J.E. Braun., *A review of literature on dynamic models of vapor compression equipment*, ASHRAE Research Project 1043-RP, Report #4636-5, 2002.

[6] Chandan, V., *Modeling and Control of Hydronic Building HVAC Systems*, Dept. of Mechanical and Industrial Engineering, University of Illinois, Urbana, IL, 2010.

[7] Chi, J., and D. Didion., *A simulation model of the transient performance of a heat pump,* International Journal of Refrigeration, 5(3):176–84, 1982.

[8] Dormand, J. R.; Prince, P. J., *A family of embedded Runge-Kutta formulae*, Journal of Computational and Applied Mathematics 6 (1): 19–26, doi:10.1016/0771-050X(80)90013-3, 1980.

[9] Ding, G.L., *Recent developments in simulation techniques for vapor-compression refrigeration systems*, International Journal of Refrigeration 30, no. 7 (2007): 1119-1133.

[10] Elmqvist, H., H. Tummescheit, and M. Otter, *Object-Oriented modeling of thermo-fluid systems*, 3rd International Modelica Conference. Linkoping, Sweden, 2003. 269-286.

[11] Hosea, M.E., Shampine, L.F., *Analysis and Implementation of TR-BDF2*, Applied Numerical mathematics 20 (1996) 21-37.

[12] Hermes, C.J.L., Melo, C., Knabben, F. T., *Algebraic solution of capillary tube flows Part I: Adiabatic capillary tubes*, Applied Thermal Engineering, vol. 30 no. 5: pp. 449-457, 2010.

[13] Hermes, C. J. L., Melo, C., Knabben, F. T., 2010, *Algebraic Solution of Capillary Tube Flows. Part II: Capillary Tube Suction Line Heat Exchangers*, Applied Thermal Engineering, vol. 30, no. 5: pp. 770-775.

[14] IPCC, 2007, IPCC Fourth Assessment Report: Climate Change 2007 (AR4)

[15] IPCC, 2014: Climate Change 2014: Synthesis Report. Contribution of Working Groups I, II and III to the Fifth Assessment Report of the Intergovernmental Panel on Climate Change[Core Writing Team, R.K. Pachauri and L.A. Meyer (eds.)]. IPCC, Geneva, Switzerland, 151 p.

[16] Jain, N., *Dynamic Modeling and Validation of a Commercial Transport Refrigeration System*, Dept. of Mechanical and Industrial Engineering, University of Illinois, Urbana, IL, 2009.

[17] Lebrun, J., and J.P. Bourdouxhe, *Reference guide for dynamic models of HVAC equipment*. Project 738-TR, 1998.

[18] Lemmon, E.W., Huber, M.L., McLinden, M.O. *NIST Standard Reference Database 23: Reference Fluid Thermodynamic and Transport Properties-REFPROP, Version 9.1*, National Institute of Standards and Technology, Standard Reference Data Program, Gaithersburg, 2013.

[19] Li, H., J. Braun, and B. Shen., *Modeling adjustable throat-area expansion valves* West Lafayette, IN, USA: International Refrigeration and Air Conditioning Conference at Purdue, Paper No. 2130, 2004.

[20] Li, B., *Dynamic Modeling and Control of Vapor Compression Cycle Systems with Shut-Down and Start-Up Operations*, Dept. of Mechanical and Industrial Engineering, University of Illinois, Urbana, IL,. 2009.

[21] MacArthur, J.W., *Transient heat pump behavior: A theoretical investigation*, International Journal of Refrigeration 7(2):123–32, 1984.

[22] MacArthur, J. W., and E. W. Grald., *Prediction of cyclic heat pump performance with a fully distributed model and a comparison with experimental data, ASHRAE Transactions* 93 (Part 2) (1987): 1159-1178.

[23] Patankar, S.V., *Numerical heat transfer and fluid flow*, New York: Hemisphere Publishing Corporation, Taylor & Francis Group, 1980.

[24] Qiao, H., V. Aute, and R. Radermacher. *Comparison of equation-based and non-equation-based approaches for transient modeling of a vapor compression cycle*, West Lafayette, IN: 14th Int. Ref. and A-C Conf. at Purdue, 2012.

[25] Qi, Q., Deng S., *Multivariable control-oriented modeling of a direct expansion (DX) air conditioning (A/C) system*, International Journal of Refrigeration31(5):841–9, 1984.

[26] Rasmussen, B.P., *Control-Oriented Modeling of Transcritical Vapor Compression Systems*, Dept. of Mechanical and Industrial Engineering, University of Illinois, Urbana, IL, Oct. 2002.

[27] Rasmussen, B.P., *Dynamic modeling for vapor compression cycle – Part I: Literature review*, HVAC&R Research, v18, n 5, pp. 934-955, 2012a.

[28] Rasmussen, B.P., and Shenoy, B., *Dynamic Modeling of Vapor Compression Systems – Part II: Simulation Tutorial*, HVAC&R Research, v18, n5 pp. 956-973, 2012b.

[29] Sami, S.M., T.N. Duong, Y. Mercadier, and N. Galanis., *Prediction of the transient response of heat pumps*, *ASHRAE Transactions* 93 (Part 2) (1987): 471-490.

[30] Shah, R.K., Sekulic, D., *Fundamentals of Heat Exchanger Design,* Wiley, New York, NY, 2003.

[31] Shampine, L. F., M. W., Reichelt J. A. Kierzenka, *Solving Index-1 DAEs in MATLAB and Simulink*, SIAM Review, Vol. 41, 1999, pp. 538-552.

[32] Thermolib, 2009, http://www.eutech-scientific.de/products-services/tools/thermolib.html/

[33] Tummescheit, H. *Design and implementation of object-oriented model libraries using Modelica.* Lund, Sweden: Ph.D. Thesis, Department of Automatic Control, Lund Institute of Technology, 2002.

[34] U.S. Energy Information Administration (EIA), Monthly Energy Review, DOE/EIA-0035(2014/11), Washington, DC, November 2014.

[35] Wang, C. C., Chi, K. Y. and Chang, C. J., *Heat Transfer and Friction Characteristics of Plain Fin-and-Tube Heat Exchangers, Part II: Correlation*, Int. J. Heat Mass Transfer, 43: 2693–2700, 2000.

[36] Winkler, J. *Development of a component based simulation tool for the steady state and transient analysis of vapor compression systems.* Ph.D. dissertation, University of Maryland College Park, 2009.

[37] Zhang, W.J., C.L. Zhang, and G.L. Ding. *On three forms of momentum equation in transient modeling of residential refrigeration systems*, International Journal of Refrigeration 32: 938-944, 2009.